# *Interactive comment on* "Northern Hemisphere Contrail Properties Derived from Terra and Aqua MODIS Data for 2006 and 2012" *by* David P. Duda et al.

**Anonymous Referee #1**

Received and published: 27 October 2018

We thank reviewer #1 again for their review and comments. They have helped to improve our manuscript.

*The paper addresses important objectives: Northern Hemisphere (NH) contrail properties, in terms of coverage, optical depth, particles sizes and radiative forcing, and their changes from 2006 to 2012. It uses valuable data at high level of remote sensing expertise: multispectral MODIS data with high spatial and some temporal resolution from two polar orbiting satellites (AQUA and TERRA), from 2 years. It uses an established algorithm which has been shown to be able to detect linear contrails, at least over quasi-homogeneous surfaces (such as the oceans) and for weak traffic where overlap from various contrails and overlap with other clouds is less important.*

*The method was known to suffer from spatially variable detection efficiencies and from possibly large false detection rates from misinterpretation of linear structures in natural cirrus.*

The claim of "possibly large false detection rates from…natural cirrus" appears to be unsupported speculation by the referee. The manuscript text mentions multiple times that flight tracks are used to screen out false detections. Detection efficiency is discussed later in this reply and dealt with in more detail in a supplement to the paper.

*The overpass times of the satellites changed somewhat between the years 2006 and 2012. The changes may have some impact on the results in particular in regions with strong diurnal traffic cycles, such as over the North Atlantic.*

This statement is not correct. Terra and Aqua were designed to maintain their overpass times and have been kept in their nominal orbits ever since operations began. The reviewer is welcome to check the overpass times using NASA Langley's orbital overpass predictor at

https://cloudsway2.larc.nasa.gov/cgi-bin/predict/predict.cgi

The following table includes the local overpass times at the Equator computed for 2006 and 2012 Terra and Aqua. All of the overpasses are within a few minutes of each other and of the nominal overpass times (1030 LT for Terra, 1330 LT for Aqua).

| **Terra** | | | | |
|---|---|---|---|---|
| Date | Overpass Latitude | Overpass Longitude | Overpass Time (UT) | Overpass Time (LT) |
| 1 Jan 2006 | 0.0 N | -4.33 W | 10:45:52 | 10:28:34 |
| 1 Apr 2006 | 0.0 N | +11.14 E | 09:44:36 | 10:29:11 |
| 1 Jul 2006 | 0.0 N | -8.98 W | 11:05:21 | 10:29:25 |
| 1 Oct 2006 | 0.0 N | +9.66 E | 09:50:47 | 10:29:25 |
| 31 Dec 2006 | 0.0 N | -10.50 W | 11:11:35 | 10:29:35 |
| 1 Jan 2012 | 0.0 N | +6.46 E | 10:03:43 | 10:29:34 |
| 1 Apr 2012 | 0.0 N | +11.18 E | 09:44:58 | 10:29:41 |
| 1 Jul 2012 | 0.0 N | -8.94 W | 11:05:28 | 10:29:43 |
| 1 Oct 2012 | 0.0 N | +9.63 E | 09:50:58 | 10:29:30 |
| 31 Dec 2012 | 0.0 N | -10.45 W | 11:11:40 | 10:29:52 |
| **Aqua** | | | | |
| 1 Jan 2006 | 0.0 N | -1.99 W | 13:39:57 | 13:31:58 |
| 1 Apr 2006 | 0.0 N | -11.32 W | 14:17:58 | 13:32:41 |
| 1 Jul 2006 | 0.0 N | -6.65 W | 14:00:33 | 13:33:56 |
| 1 Oct 2006 | 0.0 N | +11.80 E | 12:47:39 | 13:34:50 |
| 31 Dec 2006 | 0.0 N | -8.22 W | 14:07:53 | 13:35:01 |
| 1 Jan 2012 | 0.0 N | +8.80 W | 12:59:46 | 13:34:58 |
| 1 Apr 2012 | 0.0 N | -11.35 W | 14:20:58 | 13:35:34 |
| 1 Jul 2012 | 0.0 N | -6.67 W | 14:02:06 | 13:35:26 |
| 1 Oct 2012 | 0.0 N | +11.93 E | 12:47:26 | 13:35:10 |
| 31 Dec 2012 | 0.0 N | -8.30 W | 14:08:30 | 13:35:18 |

As a test of how consistent the CDA was between the two satellites, we have computed the two-year relative change [(2012 – 2006)/2006×100%] in seasonal [DJF, MAM, JJA, SON] screened and unscreened contrail coverage derived from *Terra* MODIS data versus the corresponding seasonal two-year change in contrail coverage computed from *Aqua* MODIS data for each of the high air traffic regions. The results are plotted below in Figure X, which has been added to the manuscript. Figure X(a) shows a scatter plot of the relative difference in seasonal unscreened contrail coverage between 2012 and 2006 determined from *Terra* MODIS data for each of the high air traffic regions versus the corresponding 2012 minus 2006 relative difference in *Aqua*-derived unscreened coverage. Figure X(b) shows the same scatter plot with the linear regressions for each of the air traffic regions. The unscreened coverages from both satellites are well correlated with each other. The *Terra* and Aqua screened coverages are even better correlated (Figures X(c) and X(d)).

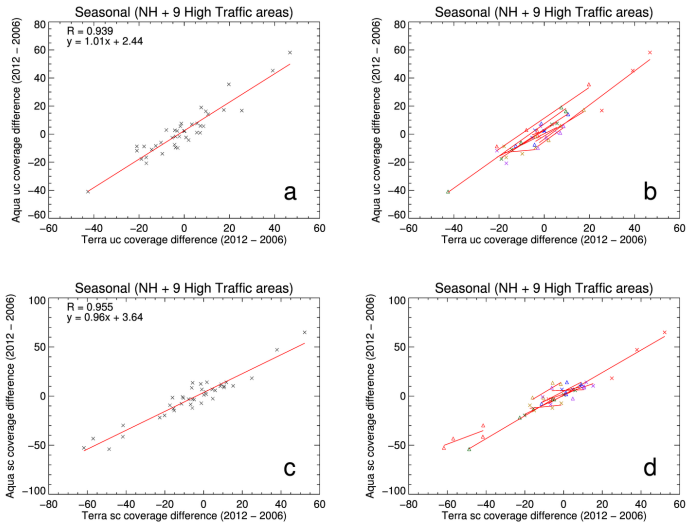


Figure X: Scatter plots of relative difference [(2012 – 2006)/2006×100%] in *Terra* MODIS-derived contrail coverage versus *Aqua* MODIS-derived contrail coverage for each air traffic region.

*For correction, meteorological data and traffic data are used, which unfortunately are different in several respect and it is not clear whether the quality of the data over the two observation periods is sufficient to allow for an unbiased comparison of the results from the two one-year periods.*

The 2006 meteorological data are from GEOS version 4 (which ended in 2007). We expect only minor differences between GEOS-4 and MERRA, the latter being built on GEOS version 5, which was found to have little impact on cloud detection except in polar regions where surface temperatures are different (see Minnis et al. https://ceres.larc.nasa.gov/documents/STM/2007-04/ce0704241020CloudsMinnis.pdf, https://ceres.larc.nasa.gov/documents/STM/2008-05/pdf/3_Minnis.CERES.5.08.pdf). Thus, we do not expect the winds to be significantly different.

*The paper comes to important conclusions: most contrails are 2 h old when detected by the satellites. That conclusion is reasonable and consistent with a few other studies (not only form their own team).*

As indicated in the text, this conclusion is also supported by the results of Vázquez-Navarro et al. (2015).

*Further the paper suggests that the NH contrail coverage increased from 0.136 % to 0.140 % in coverage or by 3 % in relative terms. Unfortunately, error estimates on these results are missing and difficult. One cannot be sure about the significance of the small*

*changes because that would require an overall accuracy better than 3 %. So, these data should be presented together with error estimates, which may be large. At present the abstract presents the coverage results as if they were accurate to 3 digits. That needs to be changed.*

We agree that the uncertainty in the screened contrail coverage estimates are probably large enough that the differences between 2006 and 2012 are not likely to be statistically significant, in large part because we have no way of evaluating the air traffic data that are critical to the screening process. We expect the detectability of contrails from year to year to be the same, but the unscreened data, while consistent with the relative changes in screened data over many regions, indicate no change in coverage. Thus, the small positive increase in screened coverage may not be meaningful. Please note that the reported coverage changes are small, thus to compute the relative change, we were required to express the coverage with at least three significant digits. We have removed mention of the 3-digit estimates from the abstract, and modified the text to acknowledge the uncertainty in the screened coverage estimates.

*Figure 1 shows the derived annual mean global distribution of detected contrail coverage. The result suggests a strong contrail maximum over the North Atlantic. The result of Figure 1 may be technically correct but the overall result does not look plausible. It contradicts many other studies in terms of the spatial distribution of contrail coverage. See all the global model studies on contrails that have been published so far since 1998 (see reviews in IPCC 1999, 2013, etc.). All of them show contrail maxima over the continents, not over the North Atlantic.*

We remind the reviewer that what we are measuring is not the same as what the models estimate. The satellites detect only some contrails, and at a specific moment in time. The models simulate all contrails (including contrails in preexisting clouds) and average over time. Also, the North Atlantic is a region favorable for the formation of persistent contrails. We have enclosed our annual-mean estimate of the frequency of persistent contrail formation (in percent) between 250 to 200 hPa (typical aircraft cruise altitudes), based on ERA-Interim reanalysis data. The PPCF is higher over the North Atlantic compared to most of Europe and CONUS.

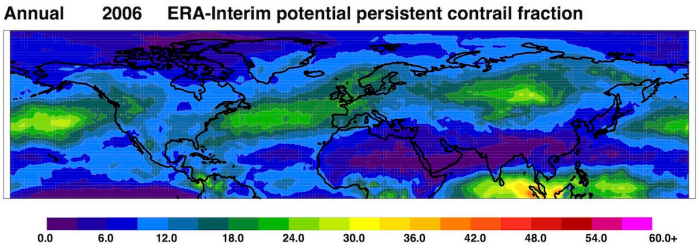

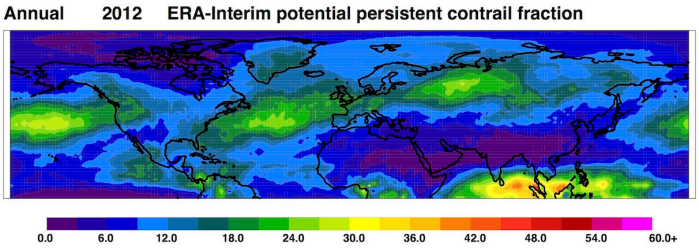


*The authors discuss traffic and potential contrail coverage computed for the given traffic using numerical weather prediction data but do not show a NH map of the absolute values of potential contrail coverage and the product of the potential coverage with traffic for comparisons. Figure 2 only shows differences in these parameters between the two annual periods. I strongly suggest to add a plot of the expected coverage and to point out that Figure 1 suffers from the spatially variable detection efficiency.*

Relating the potential and observed contrail coverage would be a good project for another paper, but it would require much additional work to determine where natural cirrus and other high clouds may impact the detection of contrails. We also note that we still do not know exactly how detectable contrail coverage relates to potential coverage and air traffic density.

*I suggest that the paper presents a table for the nine air traffic regions identified in Figure 5, comparing the observed contrail properties (coverage, RF, etc.) with computed or model-estimated contrail properties.*

Such a table would be for another study altogether. To make a **fair** comparison, the model results would have to be screened for natural cirrus and other high ice clouds that would render most contrails invisible to the satellite. In addition, model-based estimates would have to consider the detectability limitations of the satellite imagery and the temporal and spatial sampling of the satellite observations. This would be a far bigger task than due for this paper.

*The authors cite Meyer et al. (2002, JGR, doi: 10.1029/2001jd000426) but the list of references misses this paper. Another paper, Meyer et al (2007, Int. J. Rem. Sens., doi: 10.1080/01431160600641707) also discussed contrail coverage,*

The missing Meyer references have been added to the text.

*and their Table 1 shows what I was looking for: a comparison between observed and computed contrail coverage over various regions of the world. Of course, nowadays such a comparison can be made far better than >10 years ago, and other model results became available in the literature.*

See discussion of model comparisons above.

*The discussion o altitude changes is not convincing. There is no reasonable and testable argument given for why the mean cruise altitude of air traffic should have been increasing by 0.26 km or 0.79 km over the NH or over the Pacific during the just <6 years since 2006, except that two data sets of different origin indicate this. I suggest skipping this discussion and the related Table 2.*

We observe that the technique for reporting heights is the same over CONUS in both datasets, thus the 0.3 km increase in that region is very likely to be real. The differences over other areas may be less certain, but if the CONUS heights are right, the others are probably in the same direction. The height information is used in the retrieved contrail properties (optical depth, effective particle size, and radiative forcing), so we believe it must be included in the paper. To clarify the discussion in the text, we have added that the change in mean cruise altitude was a reported change.

*The values given for global radiative forcing do not yet contain error bounds for possibly underestimated contrail coverage over the continents. I suggest that the authors estimate possible underestimates over the continents (e.g., from the mentioned comparison to model data) and use such estimates to derive an upper bound on contrail coverage or RF from their data.*

This study focuses on our satellite-based estimates. An estimate of RF over the continents has already been included in the paper based on the contrail cirrus estimate. We also have unpublished work that can provide an annual-mean corrected (for background inhomogeneity) contrail coverage estimate for the 2006 data. This estimate is based on a visual analysis that we performed on the 2006 data, including an inhomogeneity correction based on Meyer et al. (2002). A brief summary of that work has been included as a supplement. The correction increases the Terra NH-mean coverage by 25 percent (from 0.136 to 0.170%), which would thus increase the overall linear contrail RF by an equal proportion. (The corrected 2006 Aqua coverage is 0.169%.) The corrected Terra coverage shows that the maxima in CC is now over CONUS and Europe, although the corrected Aqua coverage still has a maximum over the North Atlantic due to the decrease in detectability of linear contrails over the continents during the afternoon. We are not able to re-do the visual analysis for the 2012 coverage due to the considerable labor requirements. Assuming the same correction as for 2006, the corrected 2012 Terra (Aqua) coverage increases to 0.178% (0.185%).

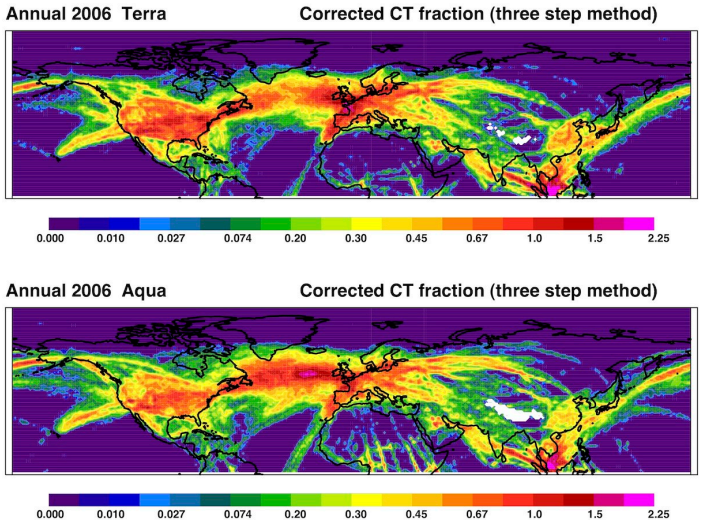


*The discussion of "interannual" changes should be reduced. There is no significance in the detected "interannual variability" if only 2 years are considered. The best one could do is to report differences between the two years. So instead of saying the cover changed from 2006 to 2012, they should say the data from 2012 and 2006 show differences, but should add that the differences can have many reasons, including true contrail changes, humidity changes, traffic changes, changes in the observation method, etc.*

As the first sentence of the abstract states, this study compares contrail properties derived from satellite data measured during 2006 and 2012. We believe it is clear to the reader that we are discussing changes in observed contrail properties between the two years, and that several factors may be causing the differences. The use of language such as "contrail coverage changed from 2006 to 2012" is simply a report of a difference between results from two years, not a declaration of absolute accuracy in measurement. As for the use of "interannual", we have removed some unnecessary instances of the word (mostly in the figure captions), and used other phrases when possible to describe "interannual". We note that the phrase "interannual variability" only occurs once in the manuscript, where the future possibility of adding an additional year of contrail properties is discussed.

*I encourage the authors to carefully revise the paper and to publish the facts and the data sets, with proper comparisons to model results, more restrictive conclusions, and self-critical discussion.*

The referee's comments here are not clear to us. What is meant by "publish the facts and the data sets"? What facts and data sets, the entire two-year, two-satellite set of MODIS imagery? A release of the source code and data sets is not

reasonable. It is not feasible to upload the hundreds of gigabytes of satellite data processed in this study. The source code is experimental and not easily implemented by someone unfamiliar with the programs. In addition to contrail detection, we also retrieve contrail optical properties and radiative forcing with additional code and processing systems.

# *Interactive comment on* "Northern Hemisphere Contrail Properties Derived from Terra and Aqua MODIS Data for 2006 and 2012" *by* David P. Duda et al.

**Anonymous Referee #2**

Received and published: 16 November 2018

We thank reviewer #2 for their review and comments. They have helped to improve our manuscript.

*The study involves a very relevant comparison of satellite contrail retrieval outputs by contrasting annual averages from two years in terms of differences in traffic, coverage, optical depth, and particle size. Nevertheless, this comparison is confounded by differences in altitude, meteorology and background characterisation techniques. I would strongly suggest that all comparisons in the study are performed separately for each variable, while keeping all others constant. I believe that this should be easily done with the data already available in the study, as this would greatly expand the applicability of the results to a wider community.*

*The title of the article should reflect the fact that this is a comparison of two years of contrail retrievals with respect to variables not necessarily linked to "interannual variability", as it is the case for traffic and altitude changes between the two years. I would make the following specific suggestions:*

Following the suggestion of anonymous referee #1, we have already revised the title of the paper to "Northern Hemisphere Contrail Properties Derived from Terra and Aqua MODIS Data for 2006 and 2012".

*a) Provide an estimate of the uncertainties and differences in the calculated potential contrail coverage between the ECMWF and MERRA data. This will allow modellers to inform their choice of data base and help to quantify the uncertainties linked to the calculated contrail coverage. It would be useful to give these differences in PPCF from the ECMWF and MERRA as maps and latitudinal and global averages. Depending on the temporal pattern of the differences, the results might need to be presented as seasonal or monthly averages.*

Currently, any estimate of linear contrail coverage using the PPCF from the two meteorological re-analyses and air traffic would be very uncertain. Although the annually-averaged spatial patterns of PPCF calculated from ERA-Interim and MERRA are generally similar, the absolute values differ by nearly a factor of two. (Notice the difference in the scale in the following annual means.)

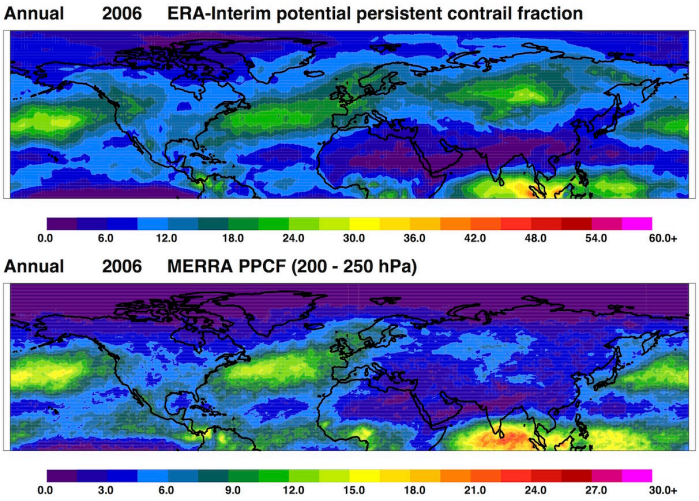


It would complicate an already long manuscript to present maps of the monthly or seasonally varying PPCF in the paper. However, we agree that a comparison of the year-to-year variation of seasonal PPCF from both re-analyses with the corresponding changes in contrail coverage would be valuable. To simplify the analysis, we computed the two-year relative change [(2012 – 2006)/2006×100%] in seasonal [DJF, MAM, JJA, SON] screened and unscreened contrail coverage versus the corresponding seasonal two-year absolute (2012 - 2006) change in PPCF computed from both MERRA and ERA-Interim data. The year-to-year changes in coverage were calculated for each season in each of the nine high air traffic regions plus the NH and plotted versus the corresponding changes in PPCF.

The following figures (Y and Z) have been added to the manuscript. Figure Y(a) shows a scatter plot of the relative difference in seasonal unscreened contrail coverage between 2012 and 2006 determined from *Terra* MODIS data for each of the high air traffic regions versus the corresponding 2012 minus 2006 absolute difference in PPCF computed for each season and each air traffic region from the MERRA re-analysis data. Figure Y(b) shows the same scatter plot with the linear regressions for each of the air traffic regions. Note two outlier plots: the red crosses represent the North Atlantic region while the brown triangle regression with the anti-correlation between coverage and PPCF represents the NE Pacific region. In Figures Y(c) and Y(d), the screened coverage and MERRA PPCF are essentially uncorrelated due to the additional outlier relationships between screened coverage and PPCF (red triangles represent Europe/Latin America corridor; green triangles represent HI/CONUS corridor). Figure Z shows similar relationships between the seasonal *Terra* MODIS-derived contrail coverage and

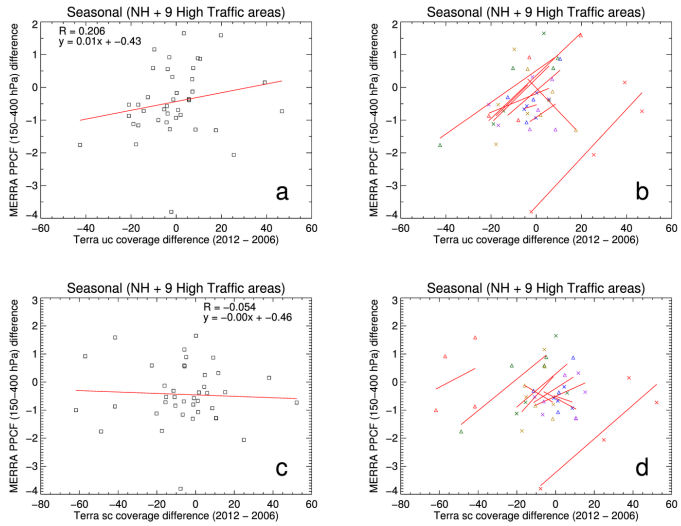


Figure Y: Scatter plots of *Terra* MODIS-derived contrail coverage versus PPCF computed from MERRA re-analyses of the upper troposphere (150 – 400 hPa).

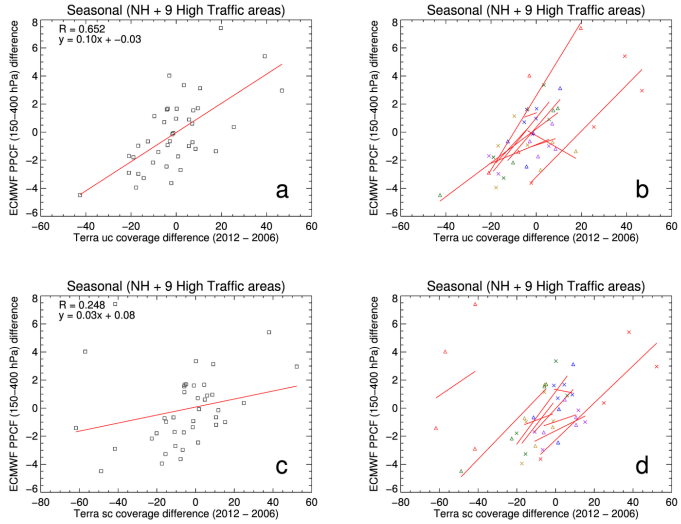


Figure Z: Scatter plots of *Terra* MODIS-derived contrail coverage versus PPCF computed from ECMWF re-analyses of the upper troposphere (150 – 400 hPa).

the ERA-Interim-based PPCF, although the correlations are stronger than for the MERRA data. Overall, the correlations are better for the PPCFs computed from the ERA-Interim re-analyses, and for the unscreened coverage. The differences between the unscreened coverage and the screened coverage scatter plots suggest that the nature of the air traffic data between 2006 and 2012 may have changed for the Europe/Latin America and the HI/CONUS air routes. The North Atlantic air route appears to be an outlier from the other air traffic regions in both the screened and unscreened contrail coverage scatter plots. Because very few unscreened contrails in the North Atlantic region are screened out by the flight track screening, the similarity between the unscreened and screened results would be expected. The shift of the North Atlantic regression to the right of the other regions suggests that contrails might have been more easily detected in the North Atlantic during 2012. The standard deviation of the background 12-μm brightness temperature, which is known to affect the detectability of linear contrails by the CDA, decreased by about 10% in 2012 compared to 2006 in the North Atlantic region, which may account for some of the discrepancy. (In contrast, however, the HI/CONUS region had a decrease in the 12-μm BT variability of 11 – 15% between 2006 and 2012, but the unscreened coverage changes are in more agreement with the other air traffic regions. The other air traffic regions generally had background heterogeneity changes of less than 5% between the two years.) In addition, the magnitude of the discrepancy between the North Atlantic and the other air traffic regions is noticeably larger in the MERRA-based plots. It appears that there is greater uncertainty between the MERRA- and ECMWF- derived PPCF in this region between 2006 and 2012 than in other regions.

*b) It would be useful to complement Table 2 with maps of temperature and PPCF, but in this case contrasting the differences between 2006 and 2012. This will make it easier to understand the latitudinal dependence of PPCF on temperature changes and validate them by screened CC retrievals. The maps, again, should probably correspond to representative seasons or months, depending on their variability between the two years.*

Please note that the contrail temperatures used in the contrail property retrievals are based on annual means that relate the average contrail altitude/pressure height with temperature. Thus, the inclusion of monthly or seasonal maps of temperature changes is detail beyond what we intended for this study.

*c) In order to explain the differences between the two years in terms of the change in altitude, it should be easy with your available data to perform PPCF calculations using the actual altitudes and present them in a map together with traffic differences and their resulting CC. This will provide an observational measure of the relative dependence of CC on altitude. The comparisons will require to first keep traffic volume constant in order to assess the altitude dependence only, and then assess the contribution from traffic volume differences.*

*I believe that this altitude-dependence assessment will provide extremely useful information to link model outputs and climatological data on how the optical depth and De can be prescribed in terms of ambient temperature, please do not exclude this section from the manuscript.*

The determination of how CC relates to altitude/pressure is not clear from the data. When we plotted the two-year differences in contrail coverage (both screened and unscreened) for each season and each air traffic region with the corresponding two-year change in PPCF *at each pressure level*, none of the plots showed a strong correlation between CC and (one pressure level) PPCF. A stronger correlation was only evident when we used the two-year change in PPCF computed throughout the upper troposphere (150 – 400 hPa). This result at least shows that the relation between satellite-observed CC and re-analysis-derived PPCF with altitude is complicated and the topic of another study.

*d) It is not clear to me how contrail radiative forcing was calculated, this should be appropriately described in the manuscript.*

Text has been added to section 2.3 to describe the calculation of the contrail radiative forcing.

*e) The suggested analyses should provide a way to discriminate the sources of the differences in retrieved CC between the two years. For these analyses the background characterisation must therefore be somehow be kept constant so it does not affect the conclusions.*

*I believe that with these additions the paper will make a much more significant contribution to the way in which we understand contrail retrievals from satellites and guide the use of retrieved atmospheric and contrail data in contrail models.*

It is not clear what the reviewer is requesting here in terms of "background characterization". We agree that the reviewer's suggestions are helpful in minimizing the unavoidable effects that result from having to use some different data sets in the two years of analysis.

*Pg 2 ln 28, delete "and"*

The extra "and" has been deleted.

# *Interactive comment on* "Northern Hemisphere Contrail Properties Derived from Terra and Aqua MODIS Data for 2006 and 2012" *by* David P. Duda et al.

**Anonymous Referee #3**

Received and published: 22 November 2018

We thank reviewer #3 for their review and comments. They have helped to improve our manuscript.

*General comments: This paper compare the linear contrail coverage, optical property, and radiative forcing data over the Northern Hemisphere (NH) 2006 and 2012 year of Terra and Aqua MODIS imagery. In the section of Methodology, authors said they employ the optimized CDA algorithm with different contrail masks, while the mid-range Mask B have the best overall balance between falsely detected and missed contrails.*

*Specific comments: Different with other two Referees, I have such the following specific suggestions: 1. The CDA and modified CDA had made lots of great works, and the detection efficiency raise up all the time. But authors did not release their source code and date sets. It is different to compare their result for other scientists, for example different contrails detection method with the same datasets, or the CDA and modified CDA with other satellite imagery.*

A release of the source code and data sets is not reasonable. Relatively few contrail detection papers have been published due to the difficulty in processing such large satellite datasets. It is not feasible to upload the hundreds of gigabytes of satellite data processed in this study. The source code is experimental and not easily implemented by someone unfamiliar with the programs. In addition to contrail detection, we also retrieve contrail optical properties and radiative forcing with additional code and processing systems.

*2. Two new masks (labeled Mask D and E) were developed to estimate contrail cirrus coverage. Please illustrate the difference among different masks. How the post-processing method detect non-linear contrail cirrus missed by the CDA, wehther could be verified with Geostationary satellite in local region?*

An example of Mask D and E is presented in Figure 11. A description of the post-processing method and the reasoning used to estimate contrail cirrus coverage appears in Section 2.1. As described in the text, visual analysis by a human observer of several MODIS granules was used to verify and to optimize the post-processing method. The visual analysis was limited due to the labor-intensive nature of the assessment, which required several rounds of analysis while the post-processing method was developed. We expect that loops of geostationary satellite data would be helpful in future development of the contrail cirrus mask, but this

would require another study altogether.

*3. Author said that the total contrail cirrus coverage visible in the MODIS imagery may be three to four times larger than the linear contrail, how to make sure that.*

The total contrail cirrus coverage estimate is based on the results of Masks D and E. The assessment of contrail cirrus remains an open problem and requires additional study. We have already included text in the manuscript explaining that the estimates are preliminary and require additional refinement. In the final section of the paper, we have proposed how the contrail cirrus estimates may be improved by using loops of geostationary data to define contrail cirrus coverage better.

*I suggest the authors could release the source of contrail detection and the data sets, while carefully revise the paper with more comparisons and more restrictive conclusions. With the source code and data sets as supplementary materials , I think more and more scientists will participate the research how the contrails impact radiative forcing, even climate change.*

Please see the comment above regarding the release of the satellite data sets.

# Northern Hemisphere Contrail Properties Derived from Terra and Aqua MODIS Data for 2006 and 2012

David P. Duda[1], Sarah T. Bedka[1], Patrick Minnis[1], Douglas Spangenberg[1], Konstantin Khlopenkov[1], Thad Chee[1], and William L. Smith, Jr.[2]

[1]Science Systems and Applications, Inc., Hampton, VA 23666-5986, USA
[2]NASA Langley Research Center, Hampton, VA 23681-2199, USA

*Correspondence to*: David P. Duda (david.p.duda@nasa.gov)

**Abstract.** Linear contrail coverage, optical property, and radiative forcing data over the Northern Hemisphere (NH) are derived from a year (2012) of *Terra* and *Aqua* Moderate-resolution Imaging Spectroradiometer (MODIS) imagery, and compared with previously published 2006 results (Duda et al., 2013; Bedka et al., 2013; Spangenberg et al., 2013) using a consistent retrieval methodology. Differences in the observed *Terra*-minus-*Aqua* screened contrail coverage and patterns in the 2012 annual-mean air traffic estimated with respect to satellite overpass time suggest that most contrails detected by the contrail detection algorithm (CDA) form approximately 2 h before overpass time. The 2012 screened NH contrail coverage (Mask B) shows a relative 3% increase compared to 2006 data for *Terra* and increases by almost 7% for *Aqua*, although the differences are not expected to be statistically significant. A new post-processing algorithm added to the contrail mask processing estimated that the total contrail cirrus coverage visible in the MODIS imagery may be three to four times larger than the linear contrail coverage detected by the CDA. This estimate is similar in magnitude to the spreading factor estimated by Minnis et al. (2013). Contrail property retrievals of the 2012 data indicate that both contrail optical depth and contrail effective diameter decreased approximately 10% between 2006 and 2012. The decreases may be attributed to better background cloudiness characterization, changes in the waypoint screening, or changes in contrail temperature. The total mean contrail radiative forcing (TCRF) for all 2012 *Terra* observations were -6.3, 14.3, and 8.0 mW $m^{-2}$ for the shortwave (SWCRF), longwave (LWCRF), and net forcings, respectively. These values are approximately 20% less than the corresponding 2006 *Terra* estimates. The decline in TCRF results from the decrease in normalized CRF, partially offset by the 3% increase in overall contrail coverage in 2012. The TCRFs for 2012 *Aqua* are similar, -6.4, 15.5, and 9.0 mW $m^{-2}$ for shortwave, longwave, and net radiative forcing. The strong correlation between the relative changes in both total SWCRF and LWCRF between 2006 and 2012 and the corresponding relative changes in screened contrail coverage over each air traffic region suggests that regional changes in TCRF from year to year are dominated by year-to-year changes in contrail coverage over each area.

**Deleted:** are

**Deleted:** (from 0.136% to 0.140%)

**Deleted:** increased

**Deleted:** (0.134% to 0.143%)

**Deleted:** interannual

## 1 Introduction

Persistent linear contrails are aircraft-generated clouds that can form in ice-supersaturated zones of the upper troposphere and add to the naturally occurring cirrus coverage in air traffic regions. As air traffic has increased, studies (*e.g.,* Minnis et al., 2004; Eleftheratos et al., 2016) have observed increases in cirrus coverage in air traffic corridors, prompting research into the possible impacts of aviation on climate. Several studies have used satellite remote sensing to quantify linear contrail coverage (CC) and to determine the optical properties of these clouds. Mannstein et al. (1999) developed an automated contrail detection algorithm (CDA) to detect linear contrails from Advanced Very High Resolution Radiometer (AVHRR) imagery and estimated CC over Western Europe. Meyer et al. (2002) also derived CC from AVHRR data over the same region, and later over Southeast Asia (Meyer et al., 2007). Minnis et al. (2005) used the Mannstein et al. CDA and remote sensing methods to estimate contrail optical properties including optical depth ($\tau$) and effective particle diameter ($D_e$) over the north Pacific from AVHRR data. As part of ACCRI (Aviation Climate Change Research Initiative – Brasseur et al., 2016), a consistent analysis system was developed by using a single set of satellite data and algorithms to detect linear contrails (Duda et al., 2013), to retrieve their particle sizes and optical depths (Bedka et al., 2013), and to produce a concurrent analysis of the atmospheric and surface conditions that enable calculation of contrail radiative effects (Spangenberg et al., 2013) for the detected linear contrails.

Duda et al. (2013) developed a modified version of the Mannstein et al. CDA with three levels of sensitivity (Masks A, B, and C) to investigate how to distinguish linear contrails from natural background linear features. Based on subjective visual analyses by a team of observers, the mid-range Mask B was found to have the best overall balance between falsely detected and missed contrails. The contrail masks were applied to a year (2006) of 1-km *Aqua* Moderate-resolution Imaging Spectroradiometer (MODIS) imagery taken over the Northern Hemisphere (NH). To improve the detection accuracy, particularly over more difficult regions such as the Tropics where tropical cirrus streaks are common, the contrail mask results were screened using commercial flight route information to eliminate false detections in areas lacking air traffic. These results represented the first hemispherical analysis of linear CC from observations. The greatest coverage was found over the North Atlantic rather than the heaviest air traffic regions (CONUS [contiguous United States] and Europe) due to several factors, including the difficulty of detecting linear contrails when they overlap in high density air traffic regions, the increased sensitivity of the CDA over the ocean due to the relative homogeneity of the oceanic background in the thermal IR (Mannstein et al., 1999; Meyer et al., 2002), and the improved contrail detection in this region due to the broad, parallel spacing of North Atlantic flights. The NH coverage from Mask B (0.135%) was found to be less than that estimated in previous studies. Bedka et al. (2013) determined the contrail $\tau$ and ice particle $D_e$ from the MODIS data assuming that the contrails were composed of distributions of hexagonal ice columns, while contrail temperatures were estimated based on mean flight levels. The mean NH contrail $\tau$ and $D_e$ were found to be 0.216 and 35.7 μm, respectively. Both results are similar to other studies (*e.g.,* Iwabuchi et

Deleted: actual

Deleted: and

al., 2012, Minnis et al., 2005). Both $\tau$ and $D_e$ tended to decrease with decreasing contrail temperature.

The satellite-retrieved contrail properties were then used by Spangenberg et al. (2013) to compute contrail radiative effects for the detected linear contrails. Spangenberg et al. performed a cloud analysis of the same MODIS data to provide concurrent background cloud and surface parameters for contrail radiative forcing (CRF) calculations using the CC mask and optical property data. The CC and optical properties were used along with the cloud property data to compute the CRF for 4 months of *Aqua* MODIS data during 2006. The greatest net CRF occurred at night because the longwave and shortwave forcings tend to cancel each other during the day. The greatest regional forcing was found over the North Atlantic and Persian Gulf. Overlapping contrails diminished the linear contrail net CRF over areas with heavier air traffic due to missed linear contrail detections. Overall, the Northern Hemisphere net CRF was determined to be 10.6 mW $m^{-2}$ from the Mask B results, which is smaller than most climate model estimates.

Deleted: is

Although the ACCRI studies advanced knowledge of contrail radiative forcing and the impact of contrails on climate, several questions remained because of the limited temporal range of the study. More specifically, the original study could not investigate interannual changes in CC. Air traffic has increased by roughly 5% per year for many years (Lee et al., 2010), and contrail cirrus coverage is likely to have also increased. In addition, it is unclear how much year-to-year changes in upper tropospheric meteorological conditions may affect the global CC. Finally, the magnitude of non-linear contrail cirrus coverage, which cannot be detected by the CDA, is still poorly understood and has usually been studied regionally (Minnis et al., 2013; Schumann and Graf, 2013).

Deleted: interannual

To help address these uncertainties, we have derived a second year (2012) of linear contrail property and radiative forcing data over the NH from *Terra* and *Aqua* MODIS imagery. This research uses the same contrail detection methodology from the ACCRI study to extend our climatology of linear contrail properties, and examines how CC, optical properties, and radiative forcing have changed when compared to the 2006 data. A separate post-processing algorithm was also developed to estimate contrail cirrus coverage by detecting contrail-like cirrus clouds in the vicinity of the linear contrails found by the CDA, which allows us to evaluate better the impact of non-linear contrail cirrus on climate.

## 2 Methodology

### 2.1 Contrail mask

The CDA employed in this study is nearly the same as the algorithm used in Duda et al. (2013). A modified form of the Mannstein et al. (1999) method, it uses data from five (6.8, 8.5, 11.0, 12.0, and 13.3 μm) thermal infrared MODIS channels to reduce the occurrence of false positive detections. Both MODIS instruments are nearly identical, and the NASA MODIS Characterization Support Team is responsible for maintaining the calibration of both satellite sensors to the same standard (Xiong et al., 2015). As a result, the differences in the calibrated thermal IR brightness

temperatures between both satellites are small enough that the same CDA can be used on both *Terra* and *Aqua* imagery. Global aircraft emissions waypoint data provided by the FAA (similar to the data provided in Duda et al. (Wilkerson et al., 2010)) allow comparison of detected contrails with commercial aircraft flight tracks to screen out false detections. The waypoint data and U-V wind component profiles from Modern Era Retrospective Analysis for Research and Applications (MERRA, see Rienecker et al., 2011) reanalyses are combined to produce a pixel level product of advected flight tracks that are used to assign a confidence of contrail detection for the contrail mask. In addition, a new post-processing method was applied to detect non-linear contrail cirrus missed by the CDA by assuming that cirrus pixels adjacent and with similar radiative signatures to the detected linear contrails were also formed by aircraft emissions.

Between the 2006 and 2012 analyses, only a few minor changes were made to the linear contrail mask. Two unavoidable alterations to ancillary data sources were required. Because the Goddard Earth Observing System Data Assimilation System (Bloom et al., 2005) data stream ended in December 2007, MERRA reanalysis data were used to advect the contrail flight tracks. In addition, some changes were reported in the commercial aircraft waypoint data used to create the flight tracks. For the 2006 waypoint data, in regions of the NH where only flight plan data were available (generally, all areas outside of CONUS and the western North Atlantic), great circle routes were used with a random dispersion added so that the flights had a little variance. The 2012 waypoint data used the shortest-distance flight route without any variation for all non-radar flights so that most oceanic flights during each day were along virtually identical flight routes. Mask B from the original analysis is used in this study as the standard mask to determine year-to-year variations in linear contrails, because it provides the least biased contrail detection frequency based on a subjective visual analysis of contrails in a randomly selected set of 40 granules (5-minute segments of MODIS imagery) by a team of human observers (Duda et al., 2013).

Deleted: interannual

Some modifications to the contrail mask were also introduced in the processing of the 2012 data to allow for the use of the contrail cirrus post-processing algorithm. To estimate contrail cirrus coverage in the 2012 data, two new masks (labeled Mask D and E) were developed that use a two-step method to evaluate contrail cirrus coverage. The principle behind the new masks is to first detect linear contrails using a conservative mask, and then to find pixels with similar brightness temperature (BT) or brightness temperature difference (BTD) values within an arbitrary pixel distance (currently 105 pixels) from each detected linear contrail pixel, identifying these similar pixels as contrail cirrus pixels. Masks D and E were tuned to minimize respectively the false detection of surface features over desert and the false detection of tropical cirrus streamers as contrails. The post-processing algorithm was applied only to the conservative Masks D and E to minimize the possibility of adding non-contrail cirrus to the contrail cirrus estimates. For each candidate pixel in a satellite image, the algorithm uses the mean BT/BTD properties of nearby detected linear contrail pixels (currently within 50 pixels) to serve as the standard to determine which prospective pixels are similar enough to be considered contrail cirrus. The new contrail cirrus detection algorithm

contains several adjustable parameters to vary the size of the area to search for possible contrail cirrus, to vary the size of the area to look for nearby detected linear contrail pixels to serve as a comparison standard, and to change the magnitude of each BT threshold. The current version of the algorithm uses seven BT/BTD thresholds for the following combinations of thermal IR images: $13.3^i$ μm; 11 – 12 μm; 8.6 –12 μm; $12^i$ μm; (8.6 – 13.3 μm) + (11 – 12 μm) – 12 μm; (11 – 12 μm) – 13.3 μm; $6.8^i$ μm, where the *i* superscript denotes that the brightness temperature in the channel is inverted (*i.e.,* the negative of the temperature is used so that both BT and BTD images can be treated with the same procedures). Several sensitivity tests were run on a sample of 24 *Aqua* MODIS granules from 2012 and 8 *Terra* MODIS granules from 2006 covering several scene types including desert, Arctic, tropical ocean and high-air traffic regions over the North America, the North Atlantic, Europe and China. The best set of adjustable parameters was found through a process of trial and error, by visually inspecting each combination of parameters that was run, and determining the combination with the best overall results for all granules.

**2.2 Contrail property retrievals**

To determine interannual differences in contrail properties, the contrail analysis system should ideally remain as consistent and unchanging as possible. Due to the complex analysis system used to detect linear contrails and then to analyze the NH contrail properties, some changes were unavoidable. In addition to the changes in the ancillary data sources noted above, some updates and minor improvements of the background cloud characterization software were implemented. While the contrail property retrieval algorithm did not change between this study and the earlier study using the 2006 data (Bedka et al. 2013), improvements were made to the determination of background cloud properties, most notably improving the accuracy of cloud phase. These changes produced a reduction in the percentage of pixels with "indeterminate background" from several percent to nearly zero. The percentage of ice cloud backgrounds also increased, bringing the results closer to the ice cloud coverage estimated by the rigorously validated CERES cloud algorithm (CERES, 2016; Trepte et al., 2018). Several other changes were made to address software errors that had been discovered.

**2.3 Contrail radiative forcing**

The contrail radiative forcing calculations used the same procedure as with the 2006 data study (Spangenberg et al., 2013). For each contrail pixel that was assumed to be completely covered by a contrail, the radiative forcing is defined to be

$$\mathrm{CRF} = F_{\mathrm{conf}} - F_{\mathrm{con}}, \quad (1)$$

where $F_{\mathrm{conf}}$ and $F_{\mathrm{con}}$ are the upward top-of-atmosphere shortwave or longwave fluxes for contrail-free and contrail-covered conditions, respectively. The fluxes are computed using the Fu-Liou RTM (Fu and Liou, 1993; Fu et al., 1998). $F_{\mathrm{con}}$ is derived assuming an atmosphere with contrail-covered conditions where a contrail layer and background cloud, if applicable, are inserted at the relevant altitudes.

**Formatted:** No widow/orphan control, Don't adjust space between Latin and Asian text, Don't adjust space between Asian text and numbers

$F_{conf}$ is computed for the contrail-free situation for the same background conditions but without the contrail layer. Both the solar and longwave CRF are computed using equation (1), as well as the net CRF, which is the sum of solar and longwave CRF. The contrail properties, $\tau$, $D_e$, and contrail temperature, define the contrail layer for each pixel calculation. Further details of the CRF calculation are discussed in Spangenberg et al. (2013). An updated version of the Fu-Liou radiative transfer program was employed, but it is not expected to affect the computed radiative forcing significantly. The most important change to the CRF assessment would be due to differences in the determination of the background cloud properties discussed above. No CRF calculations were possible for the post-processed contrail cirrus Masks D and E due to difficulties in determining cloudiness background in situations where contrail cirrus extended over a large area.

## 3 Results

### 3.1 Contrail mask

The first and most basic parameter determined from this study is CC. The CC mask determines the amount and location of linear contrails and provides the foundation for the subsequent contrail property and radiative forcing retrievals. The results of CC Mask B for 2012 are summarized in Figure 1.

Some consistent differences appear between the *Terra* (with overpasses at approximately 10:30 and 22:30 local time) and *Aqua* (with overpasses at approximately 01:30 and 13:30 local time) coverage in 2012. For example, *Terra* coverage is greater than *Aqua* over most air traffic regions including CONUS, Europe, China, and the eastern half of the air route between Hawaii and western CONUS. *Aqua* coverage is greater than *Terra* over the central North Atlantic, portions of the Europe to Latin America (LA) air route, northern Asia, and northern Africa.

Assuming that on average the upper tropospheric temperature and humidity do not change significantly during the 3 hours between the two overpass times, then the differences found in the *Terra* and *Aqua* screened CC are mostly likely due to differences in air traffic density. Figure 2 shows the *Terra* minus *Aqua* annual mean air traffic density difference estimated at 1, 2, 3, and 4-h before the overpass times. The best match between the patterns in Figure 2 and Figure 1 appears to vary from 1 to 3 h, depending on location. Overall, good matches occur for the case where the 2012 annual-mean air traffic densities are 2 h before the overpass times, suggesting that most contrails are about 2 h old when detected by the satellite CDA. Previous studies (Duda et al., 2004, Vázquez-Navarro et al., 2015) however, have reported a contrail mean age of 1 h in contrails identified in geostationary satellite data, indicating that many mid-latitude contrails are detectable as early as 1 h after formation.

By comparing the results of this study with the 2006 data, we can examine the change in linear CC between the two years. The 2012 screened *Terra* Northern Hemisphere CC (Mask B) shows a 3% relative increase compared to 2006 data, from

Deleted: interannual changes

0.136 percent to 0.140 percent, while the 2012 screened *Aqua* coverage increased by almost 7 percent, from 0.134 percent to 0.143 percent.

An examination of the changes in screened annual mean NH CC between 2006 and 2012 (Figure 3) versus the changes in unscreened CC (Figure 4) provides some insight into how air traffic density affected the screened coverage estimations. In comparison with the screened CC, the hemispheric-mean unscreened CC changed only slightly between 2006 and 2012. *Terra* NH CC decreased 2 percent compared to 2006 data from 0.337% to 0.329%, and the 2012 unscreened *Aqua* CC increased 1 percent, from 0.312% to 0.316%. Both satellites show similar changes in the magnitude and distribution of the screened and unscreened CC between 2006 and 2012. Both the screened and unscreened CC in Figures 3 and 4 show larger increases along the North Atlantic corridor and parts of the Indian Ocean, with smaller increases over northwestern CONUS, northwestern Asia, and tropical Africa. Decreases in screened and unscreened CC from 2006 to 2012 are apparent over southern CONUS, Western Europe, and northeastern Canada. The most notable differences between Figures 3 and 4 occur in the air routes between Europe and Latin America, and between CONUS and Hawaii, where screened CC decreases between 2006 and 2012, while the unscreened CC changes are mixed.

To examine the interannual differences in CC more closely, the NH was divided into nine air traffic regions to determine where CC changes were most pronounced (Figure 5). Table 1 summarizes the relative changes ([2012 – 2006]/2006×100%) in the screened and unscreened CC (day+night) of the Northern Hemisphere for each of the nine regions.

Deleted: )

The most prominent differences between the screened and unscreened interannual CC are in the transoceanic air traffic regions (HI/CONUS, Europe/LA) and western Asia. These two transoceanic regions have significant declines in screened coverage while the corresponding unscreened coverage changes are smaller. In contrast, western Asia shows moderate declines in unscreened coverage but small increases in screened coverage. To investigate whether the differences between the screened and unscreened CC trends in these air traffic regions can be explained by changes in the air traffic density between 2006 and 2012, Figure 6 shows the difference in annual-mean air traffic density between 2012 and 2006 at 2 h before *Terra* and *Aqua* overpass time. As presented above, an examination of the differences in the *Terra* and *Aqua* screened CC for 2012 suggests that most detected contrails form approximately 2 h before satellite overpass time. Figure 6 shows that air traffic density increased over nearly all of the Northern Hemisphere between 2006 and 2012 except for the air corridor between Europe and Latin America, and over parts of the HI/CONUS corridor.

Deleted: interannual

Table 2 provides a list of the mean air traffic changes between 2006 and 2012 based on a sample of waypoint data from the nine air traffic regions. Seven of the nine air traffic regions show increases in air traffic. The largest increases occur over E Asia and W Asia. Two regions show a decrease in air traffic: a small decrease in the Hawaii to CONUS corridor, and a nearly 60 percent decrease in the Europe to LA corridor. Thus, the decrease in air traffic in these two regions results in diminished screened CC but smaller changes in unscreened CC. [The large increase in air traffic over western Asia may also explain in part why the screened

coverage remained relatively unchanged in 2012 despite the observed moderate decrease in unscreened coverage.]

Like changes in air traffic, year-to-year changes in the upper tropospheric thermodynamic state also affect the detected linear CC. To consider this possible factor, we present in Figure 7 and Table 2 the 2012 minus 2006 change in potential persistent contrail frequency (PPCF) between 200 and 250 hPa, the tropospheric layer where most of the contrail-forming air traffic occurs. The PPCF is computed using temperature and relative humidity statistics from ERA-Interim (ECMWF) reanalysis data (Dee et al., 2011), and is an indicator of how often conditions that are favorable for the development of persistent contrails occur. It is assumed that MERRA relative humidities are consistent with their ERA-Interim counterparts.

The relative differences in PPCF between 2006 and 2012 are listed in Table 2. In many of the air traffic regions, the relative differences in PPCF between 2006 and 2012 are small, suggesting that the differences between the 2006 and 2012 screened CC in those regions might be only slightly affected by the interannual changes in the thermodynamic state of the upper troposphere. However, for some regions, the year-to-year changes in PPCF are more significant, and may have played a larger role in the difference in number of detected contrails between 2006 and 2012. The PPCF changes (Figure 7) correlate with unscreened CC changes (Figure 4) over northwestern and central Asia, the Indian Ocean, southern CONUS, northern Europe and off the coast of Western Europe, Greenland, and parts of northern Canada. For the air traffic regions, the increase in screened and unscreened coverage over the North Atlantic is correlated with an increase in PPCF between 2006 and 2012, but in the Europe to LA air corridor the increase in PPCF in 2012 appears to have minimal impact on the decrease in screened CC.

For more insight into the relationship between the detected CC and PPCF, both the CC and PPCF data were sorted by air traffic region and season [DJF, MAM, JJA, SON] for both 2006 and 2012 and compared. As a test of how consistent the detection of CC by the CDA was between both satellites for both years, we first computed the two-year relative change ([2012 – 2006]/2006×100%) in seasonal screened and unscreened contrail coverage derived from *Terra* MODIS data versus the corresponding change in contrail coverage computed from *Aqua* MODIS data for each of the high air traffic regions. Figure 8a shows a scatter plot of the relative difference in seasonal unscreened *Terra* contrail coverage between 2012 and 2006 data for each region versus the corresponding two-year difference in *Aqua*-derived unscreened coverage. Figure 8b shows the same scatter plot with the individual linear regressions for each of the air traffic regions. The unscreened coverage changes from both satellites are well correlated with each other. The year-to-year changes in *Terra* and Aqua screened coverage are even better correlated (Figures 8c and 8d).

Similar scatter plots of the two-year relative change in unscreened and screened CC from *Terra* compared to the corresponding seasonal two-year absolute (2012 - 2006) change in PPCF computed from both MERRA and ERA-Interim data are shown in Figures 9 and 10, respectively. Figure 9a shows a scatter plot of the year-to-year change in *Terra* unscreened CC versus the MERRA-derived PPCF for

Deleted: interannual

Deleted: interannual

Deleted: interannual

each season and each air traffic region. Figure 9b shows the same scatter plot with the individual linear regressions for each of the air traffic regions. Note two outlier regressions in the plot: the red crosses represent the North Atlantic region while the brown triangle regression with the anti-correlation between coverage and PPCF represents the NE Pacific region. In Figures 9c and 9d, the screened coverage and MERRA PPCF are essentially uncorrelated due to the additional outlier relationships between screened coverage and PPCF (red triangles represent Europe/Latin America corridor; green triangles represent HI/CONUS corridor). Figure 10 shows similar relationships between the seasonal *Terra* MODIS-derived contrail coverage and the ERA-Interim-based PPCF, although the correlations are stronger than for the MERRA data. Overall, the correlations are higher for the PPCFs computed from the ERA-Interim reanalyses, and for the unscreened coverage. The differences between the unscreened coverage and the screened coverage scatter plots in Figures 9 and 10 suggest that the nature of the air traffic data between 2006 and 2012 may have changed for the Europe/Latin America and the HI/CONUS air routes. The North Atlantic air route appears to be an outlier from the other air traffic regions in both the screened and unscreened contrail coverage scatter plots. Because very few unscreened contrails in the North Atlantic region are screened out by the flight track screening, the similarity between the unscreened and screened results is expected. The shift of the North Atlantic regression to the right of the other regions suggests that contrails might have been more easily detected in the North Atlantic during 2012 compared to 2006. The standard deviation of the background 12-μm brightness temperature, which is known to affect the detectability of linear contrails by the CDA (Mannstein et al., 1999), decreased by about 10% in 2012 compared to 2006 in the North Atlantic region, which may account for some of the discrepancy. In addition, the magnitude of the discrepancy between the North Atlantic and the other air traffic regions is noticeably larger in the MERRA-based plots (Figures 9b and 9d) than in the ECMWF plots (Figures 10b and 10d). It appears that there is greater uncertainty between the MERRA- and ECMWF- derived PPCF in this region between 2006 and 2012 than in other regions.

The results presented here demonstrate that interannual changes in air traffic density and PPCF appear to have some influence on the change in screened satellite-detected CC between 2006 and 2012, although some of the changes between the two years are more difficult to explain, especially the large increase in screened and unscreened coverage over the North Atlantic air corridor. The increase in CC between 2006 and 2012 over the North Atlantic may be due to changes in flight altitudes in 2012 that shifted more flights into levels of the atmosphere where ambient conditions are more likely for persistent contrail formation than in 2006. Overall, the uncertainty in the screened contrail coverage estimates are probably large enough that the differences between 2006 and 2012 are not likely to be statistically significant, in large part because of the difficulty in evaluating the air traffic data that are critical to the screening process.

**Deleted:** interannual

### 3.2 Contrail cirrus coverage estimation

In addition to linear contrails, CC due to contrail cirrus would increase the overall contrail radiative forcing (CRF) as contrails spread into non-linear, overlapping cloudiness that cannot be detected by the CDA. To estimate contrail cirrus effects, Minnis et al. (2013) tracked contrails over the United States in geostationary satellite imagery and determined the properties of contrail cirrus over selected areas; visual inspection was used to insure that only contrails produced the existing cirrus clouds in each region. Overall for 21 cases, the combined linear and contrail cirrus coverage was on average 3.5 times the value determined from mask B. The contrail cirrus $\tau$ and $D_e$ values were larger than the corresponding linear contrail values.

An example of the two new masks D and E that were developed to estimate contrail cirrus coverage is presented in Figure 11 for a 5-minute *Terra* MODIS granule starting at 1210 UTC on 18 January 2012. Figure 11a shows the 11 – 12 μm BTD image, which highlights a group of linear contrails off the coast of Western Europe. Figure 11b presents the screened coverage results from Mask B, including the detected contrails off the coast, and also contrails over Great Britain, Ireland and portions of France and the Iberian Peninsula. Figures 11c and 11d display the results from Masks D and E respectively, with the linear contrails and estimated contrail cirrus shown in different colors for clarity. Both masks detect areas of diffuse cloudiness near the identified linear contrails. The optical properties of contrails approach those of natural cirrus clouds as they age (Mannstein and Schumann, 2005), thus Masks D and E can only measure nearby contrail-like cirrus, but they might also include natural cirrus. However, both masks provide a method to estimate the amount of cirrus coverage associated with linear contrails, which is nevertheless useful for observing how contrail-associated cirrus varies between different regions and satellite observation times.

Figure 12 shows the ratio between the screened linear CC from Masks D and E and the total contrail cirrus coverage computed by the algorithm. The ratio provides an estimate of how much additional cirrus coverage may be attributed to contrail cirrus formation and is referred to as the spreading factor (*SF*) in Minnis et al. (2013). As mentioned earlier, Masks D and E were developed to minimize the false detection of surface features and tropical cirrus streaks, respectively. Mask E is especially conservative to minimize the effects of tropical cirrus, and thus represents a lower bound estimate of contrail cirrus, while Mask D represents an upper bound estimate of contrail cirrus coverage. In high air traffic regions, the coverage ratio is consistently larger for *Aqua* data compared to corresponding *Terra* data for both masks, especially during the day. At least part of the daytime difference in *SF* between *Terra* and *Aqua* is due to the greater air traffic over CONUS and Europe 2 h before the *Aqua* satellite overpass time, which is when most contrails that are visible to the satellite are likely to form.

The NH-mean contrail cirrus coverage ratios during the daytime and nighttime (not shown) are similar. For *Terra* Mask D the hemispheric mean *SF* during the day (3.80) and during the night (3.82) are nearly identical, while for *Aqua* Mask D the daytime NH-mean *SF* is 4.38 and 4.30 at night. The NH-mean estimates

Deleted: ,
Deleted: it was determined from
Deleted: 8
Deleted: 8a
Deleted: 8b
Deleted: peninsula
Deleted: 8c
Deleted: 8d
Deleted: 9
Deleted: ,

of *SF* for all times (*i.e.,* day+night) and both satellites range from 4.34 to 3.80 for Mask D, and from 3.53 to 3.11 for Mask E. These estimates are roughly comparable to the mean *SF* (3.5) determined by Minnis et al. (2013).

In tropical ocean regions with significant CC [Arabian Sea, Bay of Bengal NW of Sri Lanka, South China Sea], the *SF* exceeds that of the neighboring land areas. The land/ocean discrepancy is especially visible in the *Aqua* observations and is larger during the day. The land/ocean discrepancy is not apparent at higher latitudes in either satellite and is probably the result of the BT/BTD thresholds masking out more tropical cirrus streaks over land than over ocean.

Deleted: ,

**3.3 Contrail radiative property retrieval results**

The seasonal and annual mean contrail properties retrieved from *Terra* and *Aqua* MODIS data for 2006 and 2012 Mask B screened CC are summarized in Table 3. The contrail τ retrieved from both *Terra* and *Aqua* data decreased from 2006 to 2012, both during the day (*Terra*: 14%; *Aqua*: 15%) and during the night (*Terra*: 9.3%; *Aqua*: 11%). The overall probability distribution of contrail τ was nearly the same for both years, with most contrails having τ less than 0.2 (Figure 13). Most notable in the 2012 data was the decrease in the number of large τ contrails (contrails with $\tau > 0.5$), which covered 7.5% of the 2006 dataset and only 6.25% of the 2012 dataset. The decrease might be attributed to better background characterization and/or differences resulting from the changes in waypoint screening. According to the waypoint data for 2012, the NH-mean contrail temperature decreased 1.6 K compared to 2006 due to an overall mean increase of 0.26 km in flight track altitudes. Table 2 also reports regional changes in contrail temperature. An increase in contrail height could result in thinner contrails because of the overall decrease in contrail temperature.

Deleted: 10

The 2012 *Terra* mean $D_e$ decreased 10.6% (3.6 μm) during the day and 9.6% (3.3 μm) during the night compared to the 2006 results, while for *Aqua* the 2012 mean daytime $D_e$ decreased 8.4% (3.0 μm) and the 2012 mean nighttime $D_e$ decreased 7.6% (2.7 μm) relative to the corresponding 2006 values. The number of contrails with $D_e < 24$ μm increased substantially in the 2012 data (Figure 14). The largest increase was in the 8 – 16 μm bin, where the percentage of contrails increased from 11.5% in 2006 to nearly 17% in 2012 for the *Terra* data. The number of *Terra* contrails with very large $D_e$ (>80 μm) decreased from 7.5% in 2006 to 5% in 2012, which may be attributed once again to either better background characterization or differences in flight track screening. The NH map of the difference in mean contrail $D_e$ between 2012 and 2006 (not shown) shows that the 2012 particle sizes are systematically smaller across the entire hemisphere with the largest decreases in the Arctic, confirming that the differences in retrieved $D_e$ between 2006 and 2012 likely result at least in part from changes in background characterization.

Deleted: 11

Bedka et al. (2013) indicated that a 1 K decrease in contrail temperature led to a 5.6% decrease in retrieved τ and a 1% increase in $D_e$. To investigate whether improvements and bug fixes to the background cloud property determination have affected the τ and $D_e$ retrievals, two months of 2006 *Aqua* MODIS data (Jan and Jul)

were reprocessed and compared with the original 2006 results. The two months of reprocessed *Aqua* retrievals from 2006 suggest that the updates to the contrail property retrieval code could be responsible for up to 3% of the reduction in $\tau$, and 6% of the reduction in $D_e$. These differences, coupled with the observed differences in contrail temperature, may explain most of the differences in $D_e$ and $\tau$ between 2006 and 2012.

**3.4 Contrail radiative forcing results**

The annual mean NH radiative forcing due to linear contrails (CRF) was computed for 2012 *Terra* and *Aqua* MODIS data, and is presented in Table 4 along with the 2006 results. The 12-month mean normalized (that is, the CRF assuming a CC of 100%) shortwave, longwave, and net radiative forcings for *Terra* 2012 are -4.7, 10.8, and 6.1 W $m^{-2}$. The 2012 normalized CRFs are approximately 20 percent less than the normalized CRFs computed from the 2006 *Terra* data. The decrease in normalized forcing is due in part to the decrease in mean contrail $\tau$ (Meerkotter et al., 1999) in the 2012 data. Sensitivity tests computed by Spangenberg et al. (2013) suggest that decreases in $D_e$ would also slightly diminish the longwave forcing but increase the shortwave forcing marginally, while the increase in mean contrail altitude would partly compensate for the reduced $\tau$. The normalized CRFs for *Aqua* are similar. The shortwave, longwave, and net radiative forcings for *Aqua* 2012 are -4.7, 11.5, and 6.8 W $m^{-2}$, about 20% smaller than the corresponding CRFs for *Aqua* 2006.

Changes in background scene type may also have contributed to the reduction in normalized CRF. An increase in the percentage of contrails over ice clouds (especially at night) between 2006 and 2012 (day+night: from 34.2% to 46.4% *Terra*; 31.6% to 38.9% *Aqua*) and a decrease in the fraction of clear-sky contrails (day+night: from 19.0% to 15.2% for *Terra* and 20.0% to 16.7% for *Aqua*) may have also reduced the normalized CRF because radiative forcing tends to be greater in clear skies compared to cloudy skies (Spangenberg et al., 2013).

The total contrail radiative forcing (TCRF) is computed by multiplying the normalized CRF by the contrail fraction for each image and summing for all images, thus providing a realistic estimate of contrail radiative forcing at the time of *Terra* overpasses. The 12-month mean (day+night) total shortwave, longwave, and net radiative forcings are -6.3, 14.3, and 8.0 mW $m^{-2}$ for the 2012 *Terra* data, which are 12 to 24% less than the corresponding 2006 *Terra* values. The smaller TCRF for 2012 results from the combination of an approximately 20% decrease in normalized CRF partially offset by a 3% increase in overall CC. For *Aqua*, the annual-mean (day+night) total shortwave, longwave, and net radiative forcings are -6.4, 15.5, and 9.0 mW $m^{-2}$ for the 2012 data, which are 10 to 16% less in magnitude than the corresponding 2006 *Aqua* values. The decrease in the 2012 *Aqua* TCRF results from the approximately 20% decrease in normalized CRF, partially compensated by a 7% increase in overall CC.

Table 5 presents the relative changes in total SWCRF, LWCRF, and net CRF (day+night) for the Northern Hemisphere and each of the nine air traffic regions. For both *Terra* and *Aqua*, SWCRF decreased roughly 10% over the NH. The

magnitude of the SWCRF also shrank in each of the nine air traffic regions, except for a small increase in the North Atlantic for *Terra* due to the nearly 22% increase in CC in 2012. The largest decrease in SWCRF occurred in the Europe to Latin America air route where the largest drop in CC was also reported. Larger than average declines are apparent over Europe and in the HI-to-CONUS air corridor, caused at least partially by the larger reductions in 2012 CC in those regions. Similar changes are evident in LWCRF. LWCRF decreases in 2012 compared to 2006 in all nine air traffic regions in the NH, with the largest differences occurring in the Europe to Latin America air corridor, and larger than average losses over Europe and the HI-to-CONUS air corridor. The 2012 versus 2006 differences in net CRF are similar to the changes in LWCRF because LWCRF tends to be larger than the SWCRF and thus dominates the year-to-year change in net CRF. The decreases in net CRF in 2012 are generally larger for *Terra* compared to *Aqua* except for the NW Pacific where the *Aqua* difference is slightly larger.

To demonstrate the impact of the regional changes in the screened CC between 2006 and 2012 on the regional changes in the total contrail radiative forcing, Figure 15 plots the relative change in total SWCRF and LWCRF for *Aqua* (*Terra* differences are similar) between 2006 and 2012 as a function of the relative change in screened CC for the NH and the nine air traffic regions shown in Table 5. The relative changes in both SWCRF and LWCRF between 2006 and 2012 correlate well with relative changes in screened CC over each air traffic region. The relatively high correlations suggest that the regional changes in total contrail radiative forcing from year to year are dominated by interannual changes in CC over each area. Other factors that could change contrail radiative forcing (contrail $\tau$, contrail $D_e$, or changes in the background cloud conditions) changed more uniformly across the NH between 2006 and 2012 when compared to CC.

**4 Discussion**

This study analyzes MODIS thermal IR imagery from 2006 and 2012 to investigate year-to-year changes in contrail properties over the Northern Hemisphere. The 2012 retrievals provide us some insight into the relative impact of air traffic, meteorological, and flight track screening changes on the detection of linear contrails from satellite imagery. The 2012 data show large changes in air traffic distribution across the Atlantic Ocean, including a 60% decrease in air traffic between Europe and Latin America compared to 2006 that is not reflected in the unscreened CC. Although the differences between the screened and unscreened coverage in the Europe/LA corridor suggest that flights were likely missed in the 2012 air traffic inventory, a check of multiple flight schedule data sources for the year (A. Malwitz, personal communication) showed no irregularities that would indicate dropping of flights for the Europe to Latin America region. Therefore, the overall reliability of the air traffic is assumed here to be similar to the dependability of the 2006 waypoint data. The mean reported aircraft cruise altitude on average rose by 0.26 km over the NH, with increases as large as 0.79 km over the NW Pacific region. Fichter et al. (2005) estimated that lifting flight levels globally by 2 kft (0.61

Deleted: interannual

Deleted: 12

Deleted: interannual

km) would tend to increase global CC by 6%, with most of the increase at middle and low latitudes and a decrease at high latitudes. Remarkably, the regional changes in screened CC between 2006 and 2012 match best the scenario in Fichter et al. where flights are displaced 2 kft *downward* rather than upward as suggested by the 2012 waypoint data. A comparison of the 2006 versus 2012 ECMWF PPCF changes compared to the PPCF differences computed from MERRA reanalyses (not shown) show little agreement over the North Atlantic, suggesting that details of the upper tropospheric temperature and humidity are uncertain in this region.

A comparison of the changing air traffic density patterns between the *Terra* and *Aqua* overpass times suggests that the mean age of contrails visible in MODIS imagery appears to be approximately 2 h. Thus, the CDA likely can only detect a subset of the larger, more long-lived linear contrails, which impacts the contrail properties and radiative forcing estimated in this study. Actual contrail numbers are likely larger in high air traffic regions with intersecting flights that make automated detection difficult.

Two competing effects are expected to influence contrail optical depths in the 2012 results. Flight altitudes in 2012 were generally higher than in 2006, so we would expect the contrails in 2012 were forming in colder environments with less available water vapor, thus with smaller optical depths. In 2006, significantly fewer contrails were detected over ice clouds and more contrails occurred in clear skies. Because contrails over ice clouds in both studies have the highest optical depths, and contrails in clear skies have the lowest, the impact of background cloudiness changes on contrail $\tau$ would be to counteract the effect of higher flight altitudes.

While no calculations of contrail cirrus radiative forcing were made, the total radiative forcing by contrail cirrus is expected to be proportional to the spreading factor, about 3.5 times the total CRF estimated from the detected linear contrails. For current study, a NH total net CRF of 8.5 mW $m^{-2}$ would translate to a global estimate of 4.6 mW $m^{-2}$ assuming that 93% of high altitude air traffic is within the NH (Duda et al. 2013). Thus, the global total net CRF for contrail cirrus would be about 16 mW $m^{-2}$ if contrail cirrus has the same properties as linear contrails. Minnis et al. (2013) found that the mean optical depths of contrail cirrus were 2–3 times greater (and $D_e$ 20% greater) than for adjacent linear contrails, thus contrail cirrus would have a global total net CRF on the order of 40 mW $m^{-2}$ due to the larger optical depths in contrail cirrus. Recent estimates of global total net CRF for contrail cirrus range from 50-60 mW $m^{-2}$ [Lee et al. 2010].

**5 Future Work**

Although the creation of a two-year NH contrail climatology has allowed us to determine the radiative impact of contrails more completely, further research is needed. While analyzing more years of data is desirable, the analysis was laborious such that only one year of new results was possible for this study. Regardless, we believe the analysis methods and results are unique and could be employed in future studies, including additional data if the resources were available. Neither 2006 nor 2012 had a major El Niño or La Niña event, while in 2015 a significant El

Deleted: Although

Niño developed in the Pacific Ocean, producing large-scale changes in atmospheric humidity throughout the Tropics and into the mid-latitudes. In particular, strong El Niños are usually associated with a more active sub-tropical jet over southern CONUS, increasing the probability of cirrus (and persistent contrails) in this region. From ECMWF analyses (not shown) the annual-mean PPCF over southern CONUS is 2–4% higher in 2015 compared to 2012, with even larger regional differences over northern Asia. A future study during this time period would extend the contrail climatology to three years and would improve our understanding of how interannual meteorological variability may affect contrail cirrus formation. Because this report was an analysis and description of our satellite-based contrail observation system, no comparison with model estimates of contrail coverage was included. More research is needed to compare satellite observations of contrails with such modelling estimates, but such a study would require much additional work to determine how satellite-detectable contrail coverage relates to estimates of potential coverage from meteorological conditions and air traffic density. To make a fair comparison, the model results would have to be screened for natural cirrus and other high ice clouds that would render most contrails invisible in the satellite imagery. In addition, model-based estimates would have to consider the overall detectability limitations of the imagery and the temporal and spatial sampling of the satellite observations.

Deleted: ,

The algorithm developed to detect contrail-like cirrus in this study is a preliminary attempt to define contrail cirrus. Although useful as a heuristic tool to examine how contrail cirrus detection varies between different times and locations, it requires refinement, especially over different surface backgrounds and varying viewing angles. Furthermore, the study of contrail cirrus development could be aided by the launch of next generation imagers onboard the Himawari-8 and GOES-16 satellites. These platforms can provide full disk 10 and 15-minute loops, respectively, of high-resolution multi-spectral geosynchronous imagery that would allow detailed analysis of contrail spreading by identifying individual contrails with specific flights from the waypoint database. Expanding on the analysis presented in Minnis et al. (2013), the lifecycles of a large set of identified contrails could be related to several meteorological variables (such as RHI, vertical wind, wind shear, depth of the super-saturated layer) to determine which factors influence the growth and spreading of persistent linear contrails into contrail cirrus. Such a dataset would help us improve our understanding of how contrail cirrus contributes to the observed increase in global cirrus coverage and would provide valuable data to contrail models that explicitly simulate the lifespan of contrails, thus advancing our knowledge of the impacts of contrail cirrus on climate.

Deleted: ,

**Author contribution**

David Duda prepared the manuscript with contributions from co-authors. David Duda, Sarah Bedka, and Doug Spangenberg performed the analysis of the contrail masks, contrail property retrievals, and contrail radiative forcing, respectively. Patrick Minnis conceptualized the overall research goals and aims of

the study, supervised the research project and acquired funding for the study. Konstantin Khlopenkov developed programming code for analysing the commercial aircraft waypoint data and advecting contrail tracks via the MERRA wind data. Thad Chee managed the implementation of the computer code and supporting algorithms to process the satellite data and to create the contrail masks. William Smith also supervised the research project and provided review and commentary of the manuscript.

**Competing interests**

The authors declare that they have no conflict of interest.

**Acknowledgements**

The waypoint data used for this work were provided by U.S. DOT Volpe Center and are based on data provided by the U.S. FAA and EUROCONTROL in support of the objectives of the International Civil Aviation Organization (ICAO) Committee on Aviation Environmental Protection CO2 Task Group. Any opinions, findings, and conclusions or recommendations expressed in this material are those of the authors and do not necessarily reflect the views of the U.S. DOT Volpe Center, the U.S. FAA, EUROCONTROL, or ICAO. The authors also thank three anonymous reviewers for their assistance in evaluating this paper.

**References**

Bedka, S. T., Minnis, P., Duda, D. P., Chee, T. L., and Palikonda, R., Properties of linear contrails in the Northern Hemisphere derived from 2006 MODIS observations, Geophys. Res. Lett., 40, 772-777, doi:10.1029/2012GL054363, 2013.

Bloom, S. A., et al., Documentation and Validation of the Goddard Earth Observing System (GEOS) Data Assimilation System - Version 4, *Technical Report Series on Global Modeling and Data Assimilation 104606*, 165 pp., 2005.

Brasseur, G. P., Gupta, M., Anderson, B. E., Balasubramanian, S., Barrett, S., Duda, D., Fleming, G., Forster, P. M., Fuglestvedt, J., Gettelman, A., Halthore, R. N., Jacob, S. D., Jacobson, M. Z., Khodayari, A., Liou, K., Lund, M. T., Miake-Lye, R. C., Minnis, P., Olsen, S., Penner, J. E., Prinn, R., Schumann, U., Selkirk, H. B., Sokolov, A., Unger, N., Wolfe, P., Wong, H., Wuebbles, D. W., Yi, B., Yang, P., and Zhou, C., Impact of Aviation on Climate: FAA's Aviation Climate Change Research Initiative (ACCRI) Phase II, Bull. Amer. Meteor. Soc., 97, 561–583, doi:10.1175/BAMS-D-13-00089.1, 2016.

CERES, CERES_SSF_Terra-Aqu_Edition4A Data Quality Summary, *CERES Project Document*, 30 June, 19 pp. https://eosweb.larc.nasa.gov/project/ceres/quality_summaries/CER_SSF_Terra-Aqua_Edition4A.pdf, 2016.

Dee, D. P., Uppala, S. M., Simmons, A. J., Berrisford, P., Poli, P., Kobayashi, S., Andrae,

**Formatted:** Space After: 0 pt, Widow/Orphan control, Adjust space between Latin and Asian text, Adjust space between Asian text and numbers

**Formatted:** Font: Not Italic

**Deleted:** 1002/grl.50168

**Formatted:** Font: Not Italic

U., Balmaseda, M. A., Balsamo, G., Bauer, P., Bechtold, P., Beljaars, A. C. M., van de Berg, L., Bidlot, J., Bormann, N., Delsol, C., Dragani, R., Fuentes, M., Geer, A. J., Haimberger, L., Healy, S. B., Hersbach, H., Hólm, E. V., Isaksen, L., Kållberg, P., Köhler, M., Matricardi, M., McNally, A. P., Monge-Sanz, B. M., Morcrette. J.-J., Park. B.-K., Peubey, C., de Rosnay, P., Tavolato, C., Thépaut, J.-N., Vitart, F., The ERA-Interim reanalysis: configuration and performance of the data assimilation system, Q. J. R. Meteorol. Soc., 137, 553–597. doi:10.1002/qj.828, 2011.

Duda, D. P., Minnis, P., Nyuyen, L., and Palikonda, R., A case study of the development of contrail clusters over the Great Lakes, J. Atmos. Sci., 61, 1132–1146, doi:https://doi.org/10.1175/1520-0469(2004)061<1132:ACSOTD>2.0.CO;2, 2004.

Duda, D. P., Minnis, P., Khlopenkov, K., Chee, T. L., and Boeke, R., Estimation of 2006 Northern Hemisphere contrail coverage using MODIS data, Geophys. Res. Lett., 40, 612- 617, doi:10.1002/grl.50097, 2013.

Eleftheratos K., Myhre, G., Minnis, P., Kapsomenakis, I., and Zerefos, C., Chapter 61, Manmade Changes in Cirrus Clouds from 1984 to 2007: A Preliminary Study. In: Grammelis P. (eds) *Energy, Transportation and Global Warming, Green Energy and Technology,* Springer, Cham. doi:10.1007/978-3-319-30127-3_61, 2016.

Fichter, C., Marquart, S., Sausen, R., and Lee, D. S., The impact of cruise altitude on contrails and related radiative forcing, Meteor. Z., 14, 563–572, 2005.

Fu, Q., and Liou, K.-N., Parameterization of the radiative properties of cirrus clouds, J. Atmos. Sci., 50, 2008–2025, 1993.

Fu, Q., Yang, P., and Sun, W. B., An accurate parameterization of the infrared radiative properties of cirrus clouds for climate models, J. Clim., 11, 2223–2237, 1998.

Iwabuchi, H., Yang, P., Liou, K. –N., and Minnis, P., Physical and optical properties of persistent contrails: Climatology and interpretation, J. Geophys. Res., 117, doi:10.1029/2011JD017020, 2012.

Lee, D, S., Pitari, G., Grewe, V., Gierens, K., Penner, J. E., Petzold, A., Prather, M. J., Schumann, U., Bais, A., Berntsen, T., Iachetti, D., Lim, L. L., and Sausen, R., Transport impacts on atmosphere and climate: aviation, Atmos. Environ., 44, 4678–4734, 2010.

Mannstein, H., Meyer, R., and Wendling, P., Operational detection of contrails from NOAA-AVHRR data, Int. J. Remote Sensing, 20, 1641–1660, 1999.

Mannstein, H., and Schumann, U., Aircraft induced contrail cirrus over Europe, Meteorologische Zeitschrift, 14(4), 549-554, 2005.

Meerkötter, R., Schumann, U., Doelling, D. R., Minnis, P., Nakajima, T., and Tsushima, Y., Radiative forcing by contrails, Ann. Geophys., 17, 1080-1094, doi:10.1007/s00585-999-1080-7, 1999.

Meyer, R., Mannstein, H., Meerkötter, R., Schumann, U., and Wendling, P., Regional radiative forcing by line-shaped contrails derived from satellite data, J. Geophys.

Res. 107(D10), 4104, doi:10.1029/2001JD000426, 2002.

Meyer, R., Buell, R., Leiter, C., Mannstein, H., Pechtl, S., Oki, T., and Wendling, P., Contrail observations over Southern and Eastern Asia in NOAA/AVHRR data and comparisons to contrail simulations in a GCM, Int. J. Remote Sens., 28(9), 2049–2069, doi:10.1080/01431160600641707, 2007.

Minnis, P., Palikonda, R., Walters, B. J., Ayers, J. K., and Mannstein, H., Contrail properties over the eastern North Pacific from AVHRR data, Meteor. Z., 14, 515–523, 2005.

Minnis, P., Bedka, S. T., Duda, D. P., Bedka, K. M., Chee, T. L., Ayers, J. K., Palikonda, R., Spangenberg, D., A., Khlopenkov, K. V., and Boeke, R., Linear contrails and contrail cirrus properties determined from satellite data, Geophys. Res. Lett., doi:10.1002/grl.50569, 2013.

Rienecker, M. M., et al., MERRA: NASA's modern-era retrospective analysis for research and applications, J. Clim., 114, D08125, doi:10.1029/2008JD010669, 2011.
Schumann, U. and Graf, K., Aviation-induced cirrus and radiation changes at diurnal timescales, J. Geophys. Res., 118, 2404–2421, 2013.
Spangenberg, D. A., Minnis, P., Bedka, S. T., Palikonda, R., Duda, D. P., and Rose, F. G., Contrail radiative forcing over the Northern Hemisphere from 2006 Aqua MODIS data, Geophys. Res. Lett., 40, 595-600, doi: 10.1002/grl.50168, 2013.

Trepte, Q. Z., Minnis, P., Sun-Mack, S., Yost, C. R., Chen, Y., Jin, Z., Chang, F.-L., Smith, Jr., W. L., Bedka, K. M., and Chee, T. L., Global cloud detection for CERES Edition 4 using Terra and Aqua MODIS data, IEEE Trans. Geosci. Remote Sens., submitted, 2018.

Vázquez-Navarro, M., Mannstein, H., and Kox, S., Contrail life cycle and properties from 1 year of MSG/SEVIRI rapid-scan images, Atmos. Chem. Phys., 15, 8739–8749, doi:https://doi.org/10.5194/acp-15-8739-2015, 2015.

Voigt, C. et al., ML-CIRRUS – The airborne experiment on natural cirrus and contrail cirrus with the high-altitude long-range research aircraft HALO. Bull. Amer. Meteorol. Soc., doi:10.1175/BAMS-D-15-00213.1, 2017.

Xiong, X., Wu, A., Wenny, B. N., Madhavan, S., Wang, Z., Li, Y., Chen, N., Barnes, W., and Salomonson, V., "Terra and Aqua MODIS Thermal Emissive Bands On-Orbit Calibration and Performance", *IEEE Transactions on Geoscience and Remote Sensing*, vol. 53, issue 10, pp. 5709-5721, doi: 10.1109/TGRS.2015.2428198, 2015.

Wilkerson, J. T., Jacobson, M. Z., Malwitz, A., Balasubramanian, S., Wayson, R., Fleming, G., Naiman, A. D., and Lele, S. K., Analysis of emission data from global commercial aviation: 2004 and 2006, Atmos. Chem. Phys., 10, 6391–6408, 2010.

**Table 1: Relative change in CC between 2012 and 2006 for the Northern Hemisphere and nine air traffic regions.**

| Region | *Aqua* screened | *Terra* screened | *Aqua* unscreened | *Terra* unscreened |
|---|---|---|---|---|
| NH | +6.92 % | +3.19 % | +1.15 % | -2.39 % |
| N Atlantic | +24.2 % | +21.9 % | +23.6 % | +23.9 % |
| CONUS | -5.02 % | -6.22 % | -1.93 % | -4.63 % |
| Europe | -10.4 % | -8.98 % | -11.8 % | -11.2 % |
| W Asia | +1.64 % | +0.63 % | -9.05 % | -9.66 % |
| E Asia | +5.46 % | +0.34 % | +1.91 % | -1.67 % |
| Europe/LA | -41.0 % | -51.2 % | +9.58 % | -1.54 % |
| HI/CONUS | -18.4 % | -18.3 % | -0.74 % | -6.24 % |
| NE Pacific | +4.08 % | -9.56 % | +3.89 % | +5.56 % |
| NW Pacific | +3.34 % | +6.11 % | -1.30 % | +3.92 % |

**Table 2: Changes (2012 – 2006) in annual-mean flight altitude (in km), annual-mean flight temperature (in K), and the ratio of annual-mean air traffic density between 2012 and 2006 for NH and nine air traffic regions based on a 12-day sample (15th of each month) of waypoint data from both years. Relative changes (%) in annual-mean potential persistent contrail frequency (PPCF) between 2012 and 2006 for NH and nine air traffic regions are based on ECMWF reanalysis data.**

| Region | Δkm | ΔK | 2012/2006 ratio | ECMWF PPCF diff. |
|---|---|---|---|---|
| NH | 0.257 | -1.62 | 1.250 | +3.01 |
| N Atlantic | 0.442 | -2.38 | 1.004 | +10.7 |
| CONUS | 0.298 | -1.94 | 1.053 | +2.03 |
| Europe | 0.181 | -1.00 | 1.181 | -9.60 |
| W Asia | 0.058 | -0.87 | 1.891 | -7.56 |
| E Asia | 0.144 | -1.23 | 1.721 | -8.67 |
| Europe/LA | 0.231 | -1.72 | 0.432 | +18.4 |
| HI/CONUS | 0.459 | -3.35 | 0.975 | -1.18 |
| NE Pacific | 0.625 | -2.82 | 1.084 | +1.08 |
| NW Pacific | 0.794 | -4.89 | 1.002 | -6.26 |

Deleted: Interannual changes

Deleted: interannual

**Table 3: Season-mean retrieved contrail temperature, τ, $D_e$, and average latitude of NH contrail pixels (Mask B) derived from 2006 and 2012 *Terra* and *Aqua* MODIS data.**

*Terra* 2006

| Season | Tcon (K) | | τ | | De (μm) | | Avg Lat (°) |
|---|---|---|---|---|---|---|---|
| | Day | Night | Day | Night | Day | Night | |
| DJF | 218.4 | 218.9 | 0.213 | 0.216 | 34.2 | 34.4 | N/A |
| MAM | 219.8 | 220.6 | 0.216 | 0.207 | 34.7 | 35.5 | N/A |
| JJA | 224.4 | 226.0 | 0.238 | 0.220 | 33.3 | 34.4 | N/A |
| SON | 221.1 | 221.7 | 0.217 | 0.223 | 33.3 | 33.4 | N/A |
| Annual | 221.0 | 221.5 | 0.221 | 0.216 | 33.9 | 34.4 | N/A |

*Terra* 2012

| Season | Tcon (K) | | τ | | De (μm) | | Avg Lat (°) |
|---|---|---|---|---|---|---|---|
| | Day | Night | Day | Night | Day | Night | |
| DJF | 217.1 | 217.3 | 0.183 | 0.192 | 31.2 | 31.6 | 37.0 |
| MAM | 220.9 | 222.1 | 0.186 | 0.190 | 30.2 | 31.5 | 37.4 |
| JJA | 223.1 | 224.3 | 0.208 | 0.213 | 30.0 | 30.3 | 41.9 |
| SON | 218.1 | 218.3 | 0.187 | 0.195 | 30.8 | 31.2 | 39.9 |
| Annual | 219.9 | 220.5 | 0.190 | 0.196 | 30.3 | 31.1 | 39.0 |

*Aqua* 2006

| Season | Tcon (K) | | τ | | De (μm) | | Avg Lat (°) |
|---|---|---|---|---|---|---|---|
| | Day | Night | Day | Night | Day | Night | |
| DJF | 218.7 | 219.2 | 0.214 | 0.218 | 36.1 | 35.9 | 36.5 |
| MAM | 221.5 | 222.2 | 0.215 | 0.204 | 36.6 | 36.6 | 37.4 |
| JJA | 224.3 | 225.1 | 0.232 | 0.219 | 35.4 | 35.4 | 41.2 |
| SON | 219.9 | 219.9 | 0.211 | 0.214 | 35.6 | 35.4 | 41.2 |
| Annual | 221.1 | 221.6 | 0.218 | 0.214 | 35.9 | 35.8 | 39.1 |

*Aqua* 2012

| Season | Tcon (K) | | τ | | De (μm) | | Avg Lat (°) |
|---|---|---|---|---|---|---|---|
| | Day | Night | Day | Night | Day | Night | |
| DJF | 217.2 | 217.6 | 0.178 | 0.190 | 33.4 | 33.4 | 36.1 |
| MAM | 220.9 | 221.5 | 0.181 | 0.181 | 33.2 | 33.3 | 37.6 |
| JJA | 223.1 | 223.8 | 0.205 | 0.200 | 31.8 | 32.6 | 41.7 |
| SON | 218.3 | 218.6 | 0.182 | 0.190 | 33.1 | 32.9 | 38.8 |
| Annual | 219.9 | 220.6 | 0.186 | 0.190 | 32.9 | 33.1 | 38.6 |

**Table 4: Relative change in normalized and total contrail radiative forcing between 2006 and 2012 for the Northern Hemisphere.**

| | Normalized CRF (W $m^{-2}$) | | | | | |
|---|---|---|---|---|---|---|
| | 2012 *Terra* | 2006 *Terra* | % diff. | 2012 *Aqua* | 2006 *Aqua* | % diff. |
| SW | -4.7 | -5.6 | -16 | -4.7 | -5.6 | -16 |
| LW | 10.8 | 14.0 | -23 | 11.5 | 14.2 | -19 |
| Net | 6.1 | 8.4 | -27 | 6.8 | 8.5 | -20 |
| | Total CRF (mW $m^{-2}$) | | | | | |
| | 2012 *Terra* | 2006 *Terra* | % diff. | 2012 *Aqua* | 2006 *Aqua* | % diff. |
| SW | -6.3 | -7.2 | -12 | -6.4 | -7.1 | -10 |
| LW | 14.3 | 17.8 | -20 | 15.5 | 17.9 | -13 |
| Net | 8.0 | 10.6 | -24 | 9.03 | 10.7 | -16 |

**Table 5: Relative change in total contrail radiative forcing between 2006 and 2012 for the Northern Hemisphere and nine air traffic regions.**

| Region | *Aqua* SWCRF | *Terra* SWCRF | *Aqua* LWCRF | *Terra* LWCRF | *Aqua* Net CRF | *Terra* Net CRF |
|---|---|---|---|---|---|---|
| NH | -9.8 % | -12.4 % | -13.4 % | -19.9 % | -15.9 % | -24.9 % |
| N Atlantic | -1.4 % | +0.9 % | -3.9 % | -7.0 % | -5.3 % | -14.2 % |
| CONUS | -11.7 % | -13.3 % | -18.6 % | -22.4 % | -23.3 % | -28.0 % |
| Europe | -21.2 % | -19.5 % | -25.5 % | -27.4 % | -28.3 % | -32.2 % |
| W Asia | -3.7 % | -11.9 % | -15.5 % | -20.2 % | -19.8 % | -23.8 % |
| E Asia | -14.3 % | -11.0 % | -8.3 % | -14.7 % | -4.5 % | -16.7 % |
| Europe/LA | -45.8 % | -50.0 % | -48.5 % | -61.3 % | -51.2 % | -66.3 % |
| HI/CONUS | -26.0 % | -18.9 % | -28.7 % | -32.5 % | -31.5 % | -42.7 % |
| NE Pacific | -16.4 % | -22.8 % | -16.2 % | -30.0 % | -16.1 % | -35.4 % |
| NW Pacific | -9.6 % | -19.8 % | -19.3 % | -21.9 % | -23.5 % | -23.2 % |

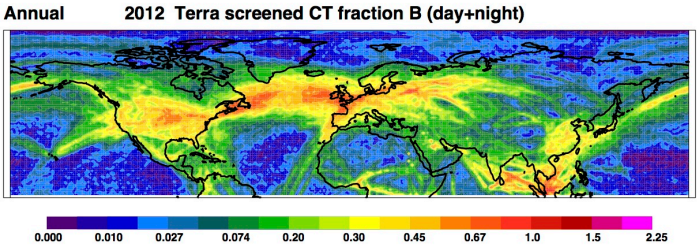

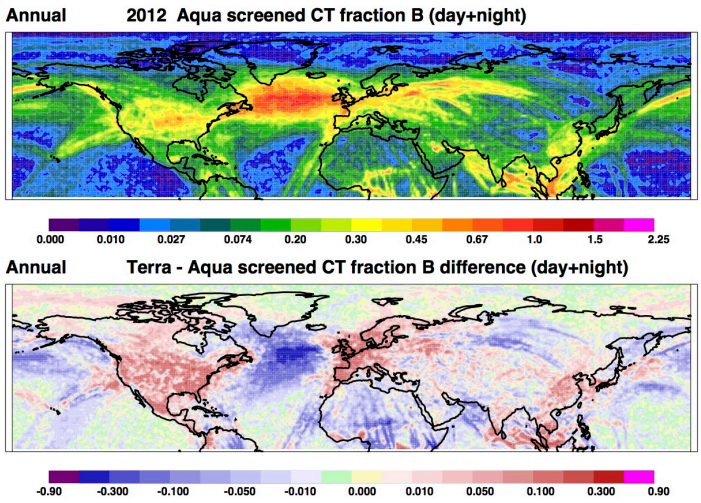


**Figure 1: The 2012 annual-mean screened NH CC from *Terra* and *Aqua* MODIS imagery (Mask B), and the difference between screened coverage for the two satellites.**

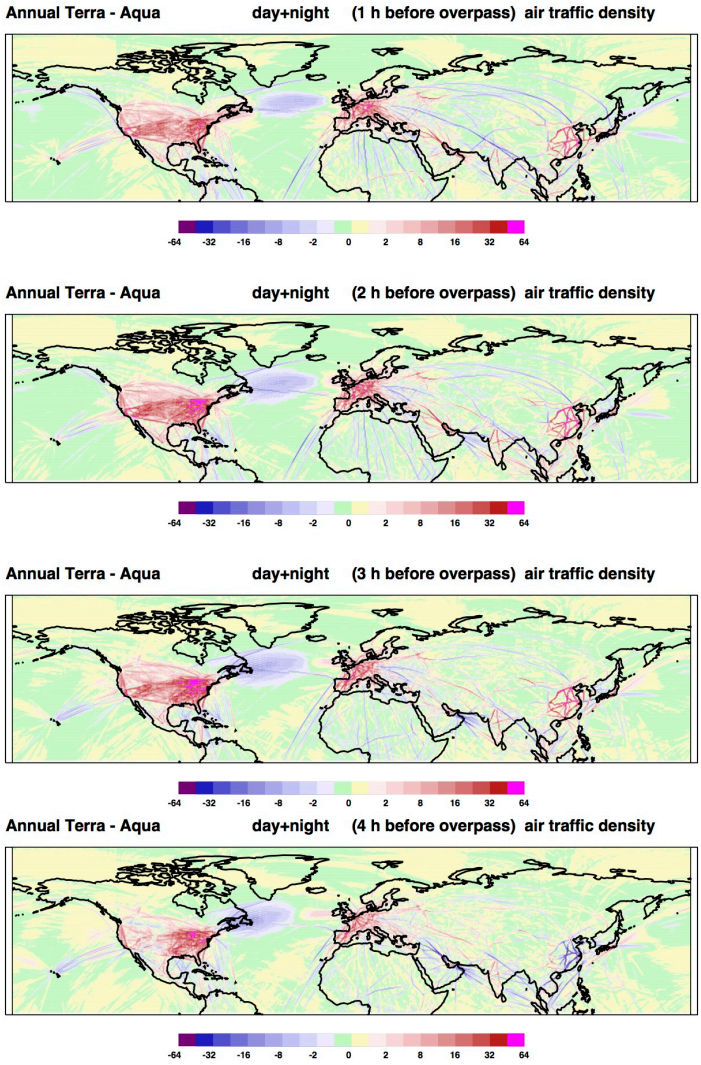


**Figure 2: The difference in the 2012 annual-mean air traffic density relative to the *Terra* and *Aqua* MODIS overpass times, for 1-h intervals from 1 to 4 h before overpass.**

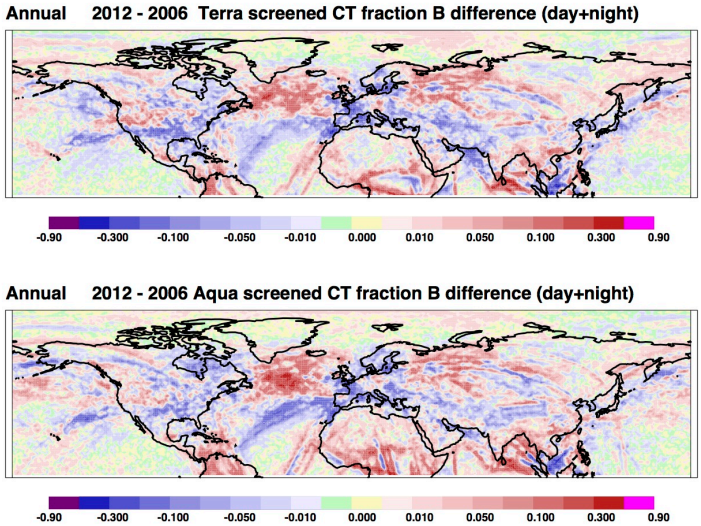


**Figure 3: Difference (2012 minus 2006) in the annual-mean screened NH CC from *Terra* and *Aqua* MODIS imagery (Mask B).**

Deleted: Interannual

Deleted: difference

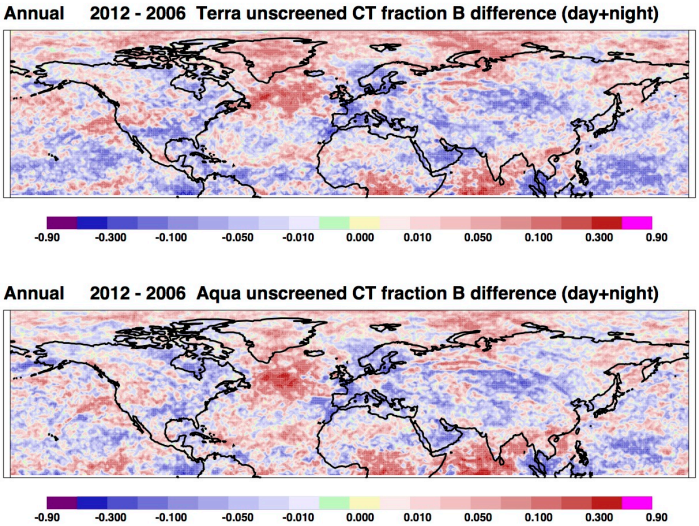


**Figure 4: Difference (2012 minus 2006) in the annual-mean unscreened NH CC from *Terra* and *Aqua* MODIS imagery (Mask B).**

Deleted: Interannual

Deleted: difference

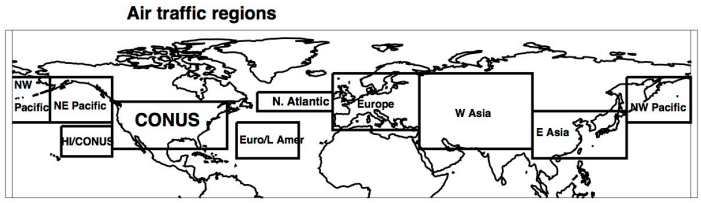


**Figure 5: Nine air traffic regions selected for study.**

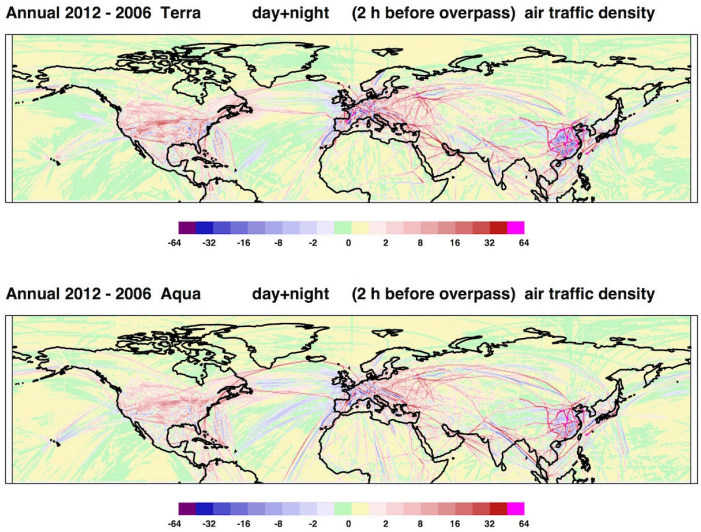


**Figure 6: Difference (2012 minus 2006) in the annual-mean air traffic density relative to 2 h before the *Terra* and *Aqua* MODIS overpass times.**

Deleted: Interannual

Deleted: difference

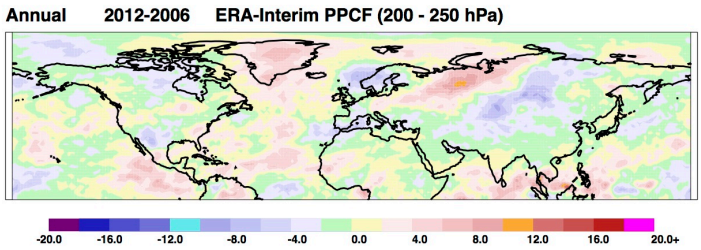


**Figure 7: Difference (2012 minus 2006) in the potential persistent contrail frequency computed between 200 and 250 hPa from ERA-Interim reanalysis data.**

Deleted: Interannual

Deleted: difference

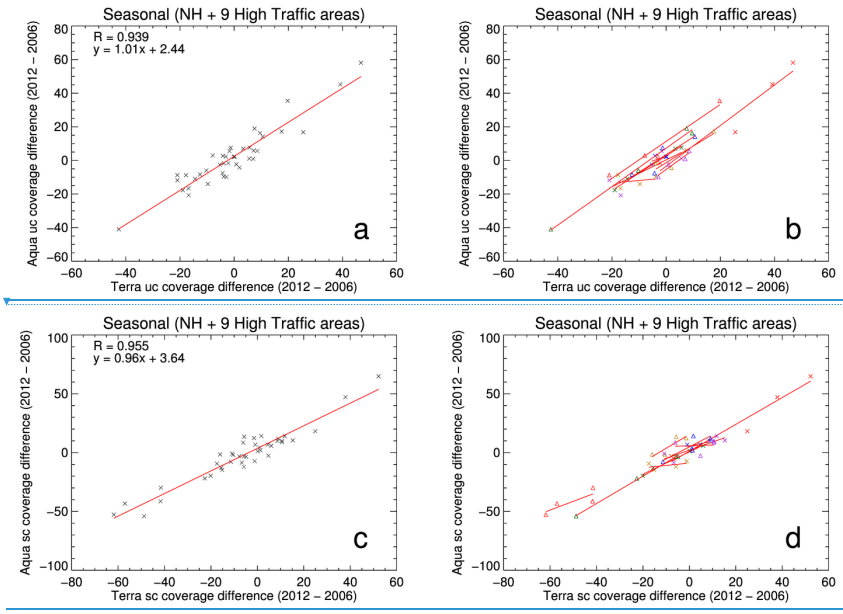


**Figure 8: Scatter plots of relative difference ([2012 – 2006]/2006 × 100%) in *Terra* MODIS-derived contrail coverage versus *Aqua*-derived contrail coverage for each air traffic region.**

**Deleted:**

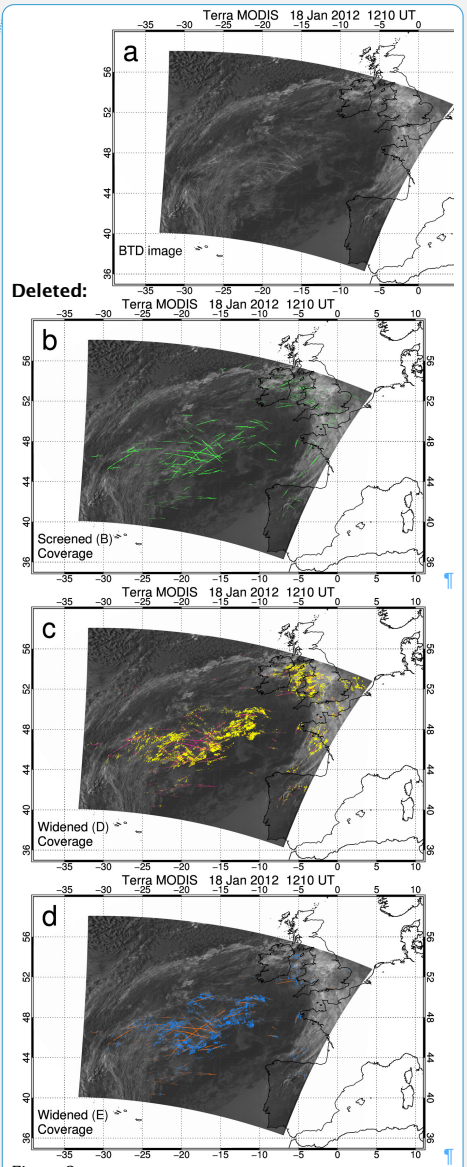


Figure 8:

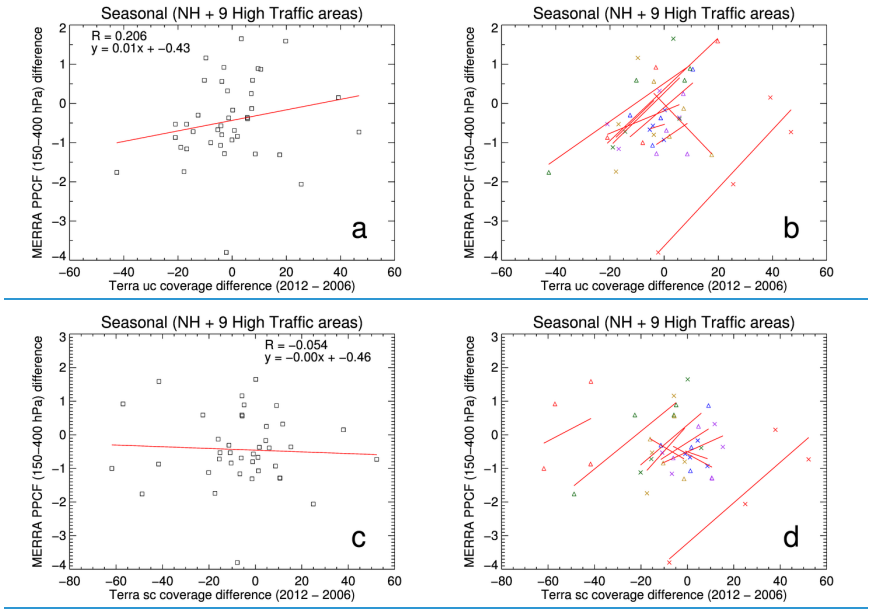


**Figure 9: Scatter plots of relative year-to-year difference in *Terra* MODIS-derived contrail coverage versus absolute (2012 – 2006) difference in PPCF computed from MERRA reanalyses of the upper troposphere (150 – 400 hPa).**

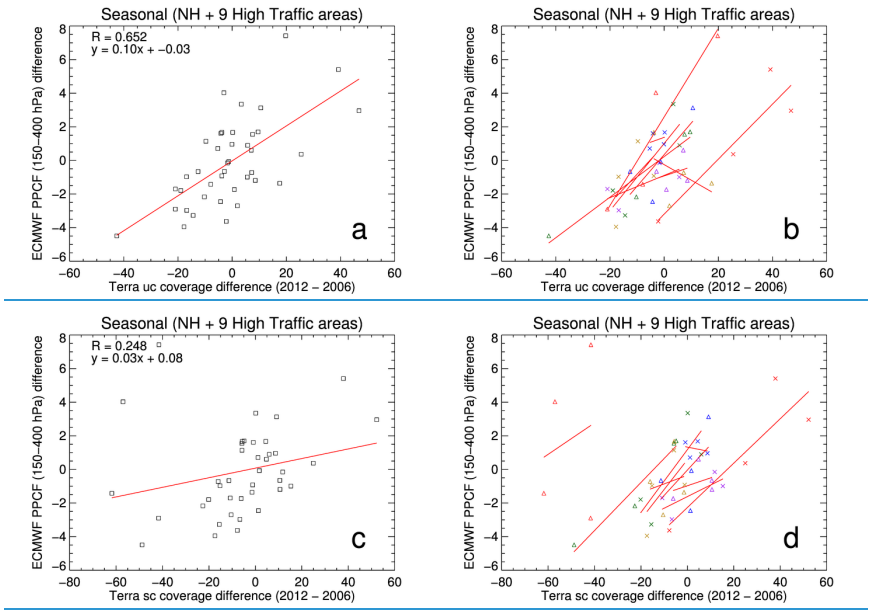


**Figure 10: Scatter plots of relative year-to-year difference in *Terra* MODIS-derived contrail coverage versus absolute (2012 – 2006) difference in PPCF computed from ERA-Interim reanalyses of the upper troposphere (150 – 400 hPa).**

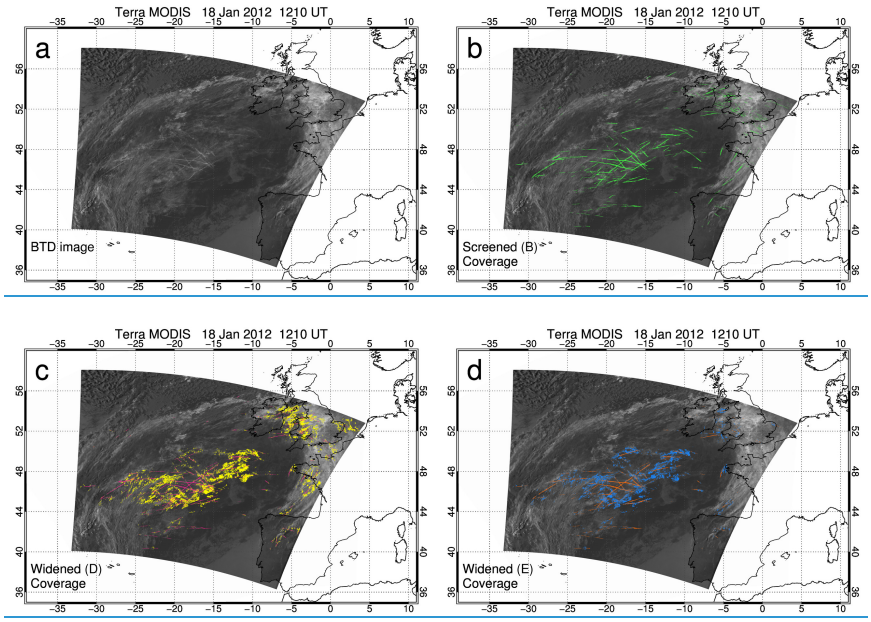


**Figure 11:** **[a] Map of 11 – 12 µm brightness temperature difference (BTD) from 5-minute *Terra* MODIS granule starting at 1210 UT on 18 Jan 2012 over the eastern North Atlantic. [b] Similar to [a], but with Mask B screened coverage in green. [c] Similar to [a] but including Mask D linear contrails in pink and contrail cirrus in yellow. [d] Similar to [c] but containing Mask E linear contrails as orange pixels and contrail cirrus as light blue pixels.**

Deleted: ],

Deleted: ],

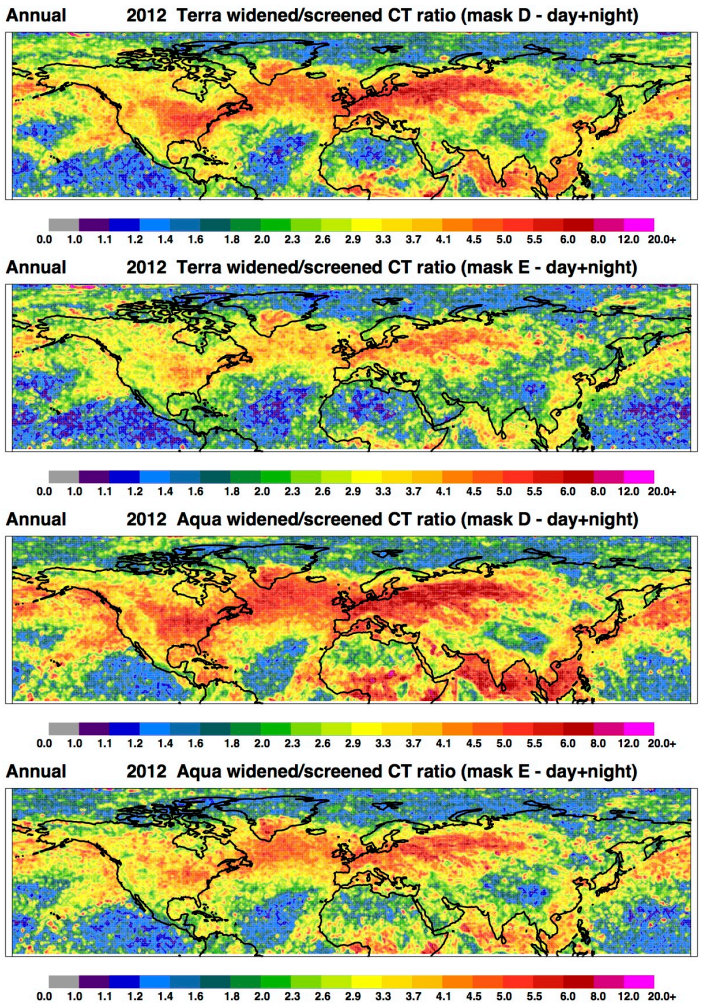


**Figure 12: The 2012 annual-mean NH widened versus screened CC ratio from *Terra* and *Aqua* MODIS imagery (Masks D and E).**

Deleted: 9

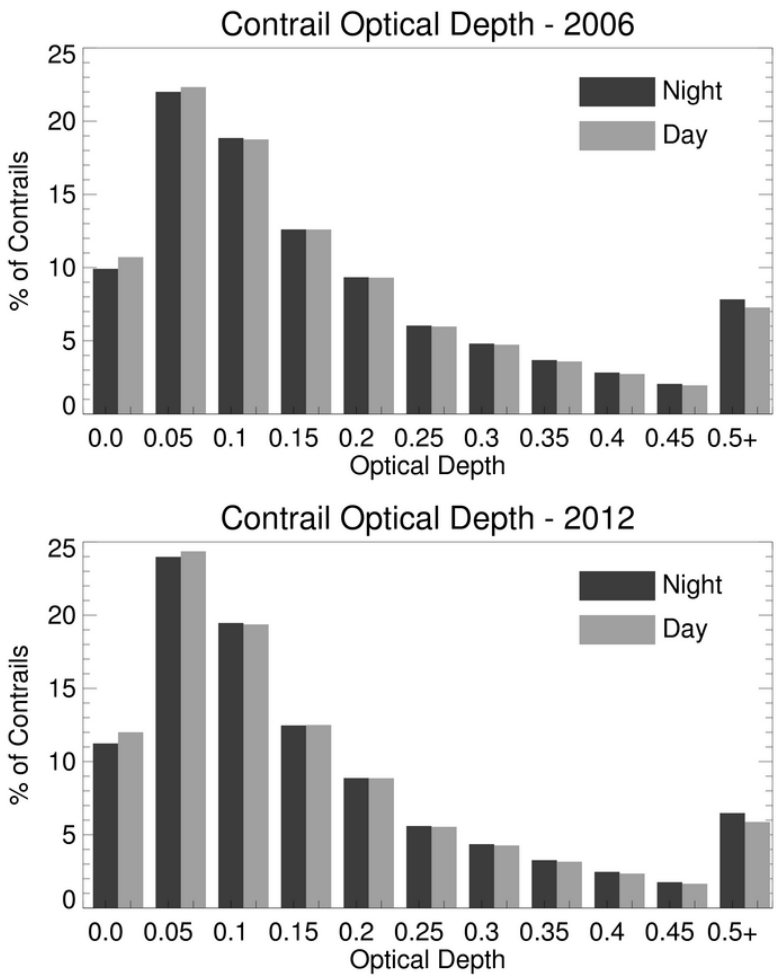


**Figure 13: Histograms of retrieved contrail τ computed from 2006 and 2012 *Terra* MODIS data.**

Deleted: 10

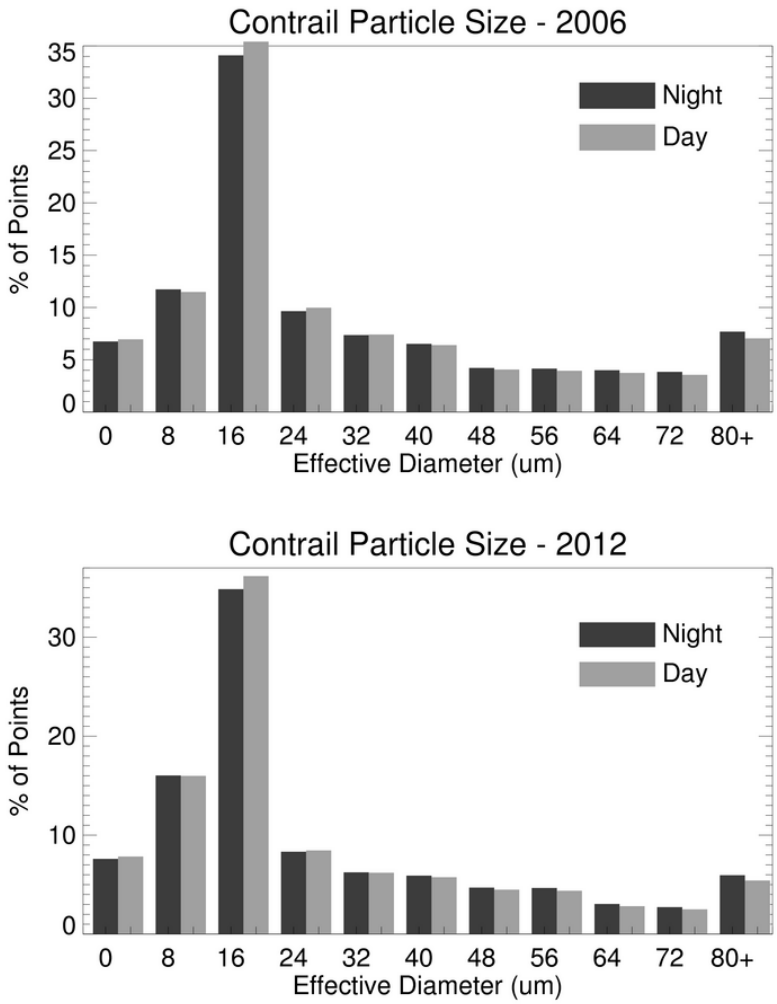


**Figure 14: Histograms of retrieved contrail $D_e$ computed from 2006 and 2012 *Terra* MODIS data.**

Deleted: 11

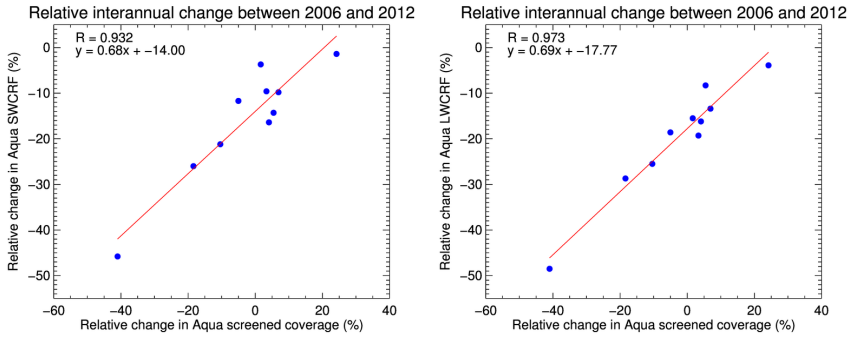


**Figure 15: Relative change ([2012 – 2006]/2006 × 100%) in the total *Aqua* contrail SWCRF and LWCRF for NH and nine air traffic regions as a function of the relative change in screened CC (day+night, Mask B).**

Deleted: 12

Deleted: )